The extended polar writhe: a tool for open curves mechanics

Christopher B. Prior
Department of Mathematical Sciences, Durham University, U.K.
Sébastien Neukirch[1,2]
[1]CNRS, UMR 7190, Institut Jean Le Rond d'Alembert, F-75005 Paris, France.
[2]UPMC Université Paris 06, UMR 7190, Institut Jean Le Rond d'Alembert, F-75005 Paris, France.

February 8, 2016

Abstract

A measure of the writhing of a curve is introduced and is used to extend the Călugăreanu decomposition for closed curves, as well as the polar decomposition for curves bound between planes. The new writhe measure is also shown to be able to assess changes in linking due to belt-trick and knotting type deformations, and further its utility is illustrated on examples taken from elastic rod parameter-continuation studies. Finally C++ and Mathematica codes are made available and shown to be faster than existing algorithms for the numerical computation of the writhe.

1 Introduction

Thin tubular bodies and ribbons are used to model the behaviour of macromolecules [35, 8, 37, 9], cables [20, 30], plant tenderils [23], magnetic flux ropes/lines [31] and topological solitons [25]. There are two important geometrical considerations required for the realistic physical modeling of such objects. The first is the prevention of self-penetration when the structure comes into self-contact whilst deforming. One of the most notable occurrences of self contact is the formation of plectonemes, depicted in Figure 1(a), which is observed in single molecule micro-manipulation experiments of the torsional response of DNA to applied moments [15, 45, 36], but also (on a vastly different scale) in twisted cables engineering [20, 30]. The second is the twisted nature of the structure. Applying rotations to a ribbon introduces twisting/winding into the system as shown in Figure 1(b). For example fluid motions at the Sun's surface injects twisting into tubular magnetic field bundles. If the ends of the ribbon are held fixed the input winding is a conserved quantity in the sense that it will stay constant when the axis deforms without its ends rotating (e.g. Figure 1(b) to Figure 1(c)), provided no cutting or passing of the ribbon/tube takes place.

Enforcing both conditions mathematically is a matter of preserving the systems topology, and mathematical measures which can be used to enforce them are known as topological constraints. The topology of thin tubes and ribbons can be quantified through a pair of curves, one representing the central axis, which is the curve that must not cross itself. The second curve represents its inherent twisting of the tube/ribbon. This twisted curve can be defined through a normal vector field attached to the central axis curve, the rate at which this field rotates determines the twist of the structure (Figure 1(d)). For tubes/ribbons which close on themselves the extent to which the ribbon links itself is an integer-valued topological invariant known as the *linking number*. The linking number $\mathcal{L}$ is invariant, i.e. it will remain unchanged for all deformations which forbid either of the curves from intersecting. It has been used in variational problems to constrain the phase space of possible closed elastic rod configurations [11, 44, 35, 19] and magnetic fields [48], as well as a constraint to categorise solitions in the Skyrme-Fadeev model [10]. In thin tube studies the tube/ribbons control of the phase space of possible configurations is achived by decomposing of the linking number into the *writhe* $\mathcal{W}$ and the *twist* $\mathcal{T}$. The writhing is a measure of the contortion of the axis curve and the twist measures the total rotation of the second curve about the tangent direction of the first. If the two curves are closed (periodic) then the three components can be linked by the Călugăreanu formula[16, 17, 39, 22]

$$\mathcal{L} = \mathcal{W} + \mathcal{T}. \tag{1}$$

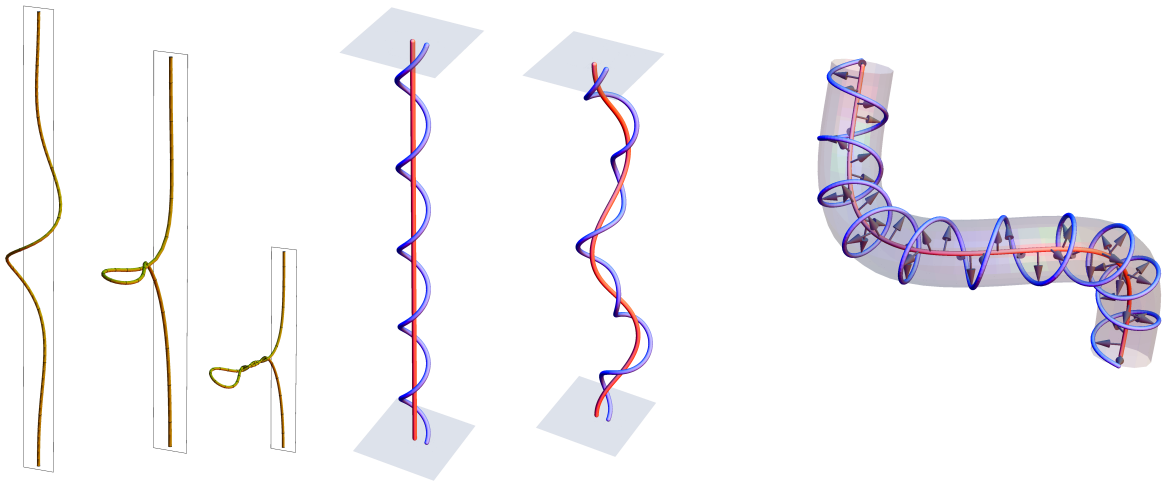

(a) (b) (c) (d)

Figure 1: (a) A sequence of deformations leading to the formation of a plectoneme as the rod comes into self contact and wraps around itself. (b) An initially flat pair of curves is subject to a number of full turns, and (c) the system is eventually allowed to deform. (d) A tube with central axis (red) and the twisted curve (blue) lying on its surface.

If the axis starts with a circular shape then $\mathcal{W} = 0$ and the $\mathcal{T}$ represents the number of turns of the ribbon/tube. As the axis deforms the total twisting is altered due to the account for rotation due to the contortion of the rods axis, this contortion is represented in (1) by the writhe. In Solar Magnetohydrodynamics (MHD) the magnetic helicity, the pair-wise average of $\mathcal{L}$ for all curves of the magnetic field, is a conserved quantity for fields whose curves do not pierce its boundary.

For open ribbons the quantities $\mathcal{L}$ and $\mathcal{W}$ are well defined, but $\mathcal{L}$ is no longer a topological invariant, even when end-rotation of a system such as the twisted ribbon shown in Figure 1(b) is forbidden. A few approaches to artificially extending the ribbon to form a closed system have been followed [3, 43, 46, 51]. However, Berger and Prior [12] introduced a topological measure called the net winding $\mathcal{L}_p$ which was derived for a pair of curves bound between two parallel planes (e.g. the system in Figure 1(b)). This includes ribbons which close within the domain and ribbons which are anchored on just one of the plane. It requires no artificial extension for its definition. The net-winding is invariant to deformations which do not allow crossings of the ribbon and for which the ribbon's ends are forbidden from turning, this second requirement limits the input of winding into the system. Moreover a quantity, termed the *polar writhe* $\mathcal{W}_p$, was introduced and an open equivalent of (1) was dervied [12]

$$\mathcal{L}_p = \mathcal{W}_p + \mathcal{T}, \tag{2}$$

the twist $\mathcal{T}$ being the same quantity as in (1). For closed ribbons $\mathcal{L} = \mathcal{L}_p$ and $\mathcal{W} = \mathcal{W}_p$ so the original Călugăreanu theorem is actually a special case of the more general decomposition (1); under the addional restriction to closed ribbons. This more general writhe-twist decomposition has been utilized in MHD studies of magnetic flux tubes in the solar corona [49, 28, 32, 41, 18, 33, 24, 50], where field lines enter the corona through the Sun's surface and are generally open curves. Magnetic (flux) tubes entering the coronal region become unstable and writhe in order to relieve the energy associated with twisting, whilst keeping the total helicity fixed. This is one of the proposed mechanisms for coronal mass ejections. In [42] it was shown that the only physically reasonable measure of the helicity of open magnetic fields is the pair-wise average of the net-winding over all curves of the field.

As it stands the (2) is not applicable to rods for which a section of the rod passes above or below the bounding planes, see Figure 2. In this note we demonstrate how the definition of the polar writhe can be extended to allow equation (2) to be applicable under such deformations (Section 3.1). This allows the

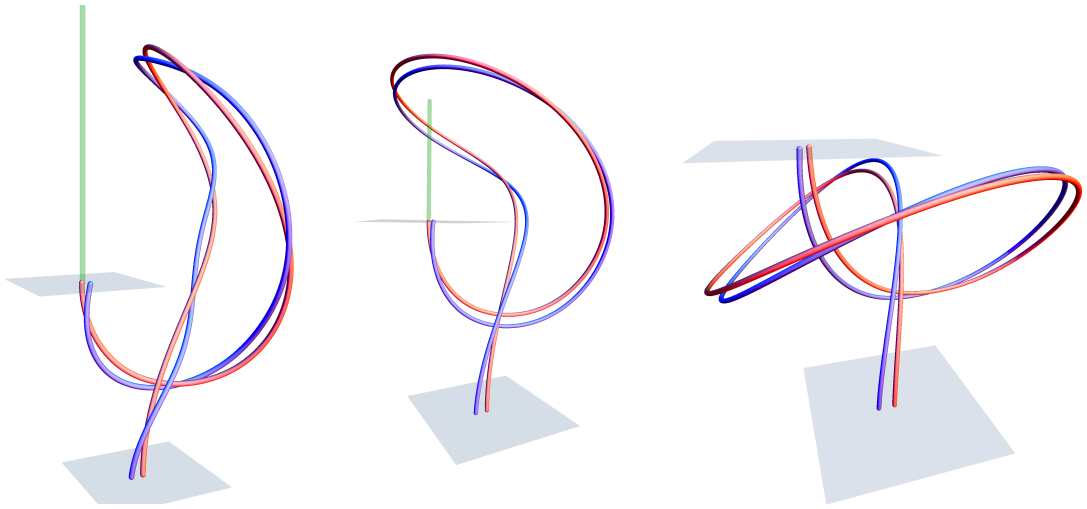

(a) (b) (c)

Figure 2: The formation of a "knotted" tube from an unknotted tube. Pulling the end planes of (a) apart would lead to a straight but twisted ribbon. Pulling on (c) would lead to a knotted ribbon which is significantly less wound (we see later the change would be -4π windings).

extension of the open form of the Călugăreanu theorem (2) to a far greater class of deformations. The issue of allowing "over-the top deformations" is somewhat complicated by the fact that open ribbons can shed integer number of twist/winding, even whilst their ends are prevented from rotating, through either the Dirac belt trick or "knotting" deformations such as depicted in Figure 2. So we cannot in general expect topological constraint of open ribbons. In sections 3 and 4 we show how the polar writhe measure can be extended to track such changes in topology whilst also measuring the continuous conversion between (polar) writhing and twisting of the ribbon.

Section 5 introduces new c++ and Mathematica codes to calculate the quantities $\mathcal{L}_p$ and $\mathcal{W}_p$ under this extension. We demonstrate its superiority in both ease of application and speed over existing algorithms which calculate $\mathcal{L}$ and $\mathcal{W}$ with closures. This is done through a number of example curve deformations generated using a simple elastic rod (thin tube) model (common to all the applications mentioned in the first line of this introduction). We should be clear that this code is designed for ribbons, a general mathematical structure defined by a pair of curves. The example calculations are simply relevant physical examples which provide a means of showcasing the efficacy and efficiency of the code, they are not intended to make any specific physical conclusions.

2 Geometry and Topology

2.1 Ribbons, Tubes and the Darboux Vector

In this note we consider oriented embedded curves in Euclidean 3-space, $[s_{\min}, s_{\max}] : \mathbf{r}(s) \to \mathbb{E}^3$, with basis $(\hat{\mathbf{x}}, \hat{\mathbf{y}}, \hat{\mathbf{z}})$ and norm $||.||$. The parametrization s may be arbitrary and, unless otherwise stated, curves are assumed to be twice differentiable with respect to s. Throughout this note derivatives will be denoted with a dash. A tube surrounding $\mathbf{r}$ can be generated using the unit tangent vector of $\mathbf{r}$

$$\mathbf{d}_3(s) = \frac{1}{\lambda}\,\mathbf{r}'(s)\,, \quad \lambda = ||\mathbf{r}'|| \tag{3}$$

and a unit vector field $\mathbf{d}_1(s)$ which lies in the normal plane of $\mathbf{d}_3$, that is $\mathbf{d}_1 \cdot \mathbf{d}_3 = 0$, $||\mathbf{d}_1|| = 1$, $\forall s$. We complete an orthonormal basis with the vector product $\mathbf{d}_2 = \mathbf{d}_3 \times \mathbf{d}_1$. At a specific parameter value s the

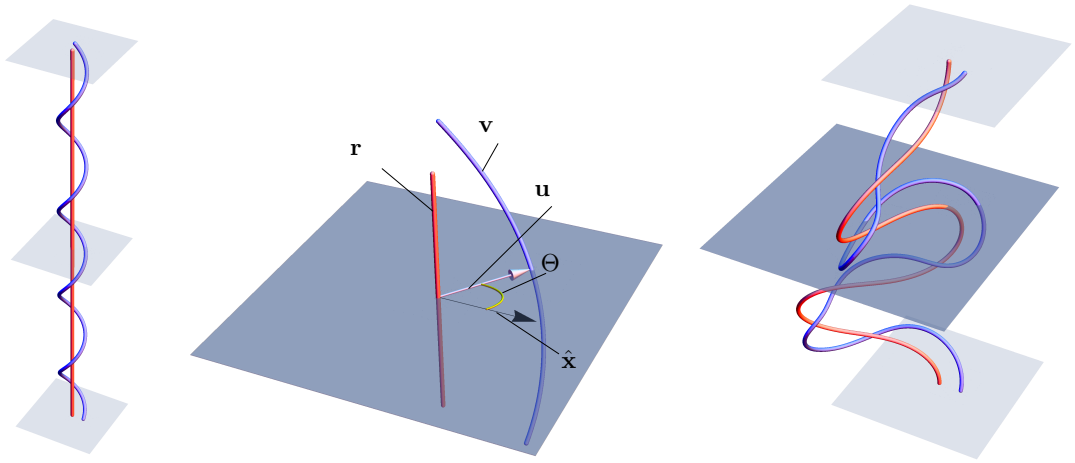

(a) (b) (c)

Figure 3: (a) shows a pair of curves simply wound. (b) depicts the mid-curve cross-section highlighted in (a) with the joining vector $\mathbf{u}$ and the angle Θ makes with the x-axis shown. In (c) we see a plane $z = \text{const}$ pierced at several points by the curves. This leads to multiple angles Θ_{ij}.

pair $(\mathbf{d}_1, \mathbf{d}_2)$ span the circular cross section $\mathcal{D}_s$, whose material points $\mathbf{p}_s$ are specified by the pair (R, ξ) with

$$\mathbf{p}_s(R, \xi) = \mathbf{r}(s) + R\,(\mathbf{d}_1(s)\,\cos\xi + \mathbf{d}_2(s)\,\sin\xi) \tag{4}$$

and $\mathcal{D}_s = \left\{\mathbf{p}_s(R, \xi)\,|\,R \in [0, \epsilon], \xi \in S^1\right\}$. The set of all $\mathcal{D}_s$ on the interval $s \in [0, L]$ constitute the tube body. The ϵ-neighbourhood theorem asserts that, if $\mathbf{r}(s)$ is a non-self intersecting curve, then there is an ϵ sufficiently small such that the tube does not intersect itself [26]. A *ribbon* can be obtained from the tube structure by choosing a fixed angle ξ, say $\xi = 0$, so that we have a pair of curves $\mathbf{r}$ and

$$\mathbf{v}(s) = \mathbf{r}(s) + \epsilon\,\mathbf{d}_1(s) \tag{5}$$

which constitute the ribbon pair. By extension if ϵ is sufficiently small the two curves $\mathbf{r}$ and $\mathbf{v}$ do not intersect. In what follows, components of a vector $\mathbf{v}$ expressed in the Euclidean co-ordinate system $(\hat{\mathbf{x}}, \hat{\mathbf{y}}, \hat{\mathbf{z}})$ will be written as (v_x, v_y, v_z), and components in the basis $(\mathbf{d}_1, \mathbf{d}_2, \mathbf{d}_3)$ will be written in sans-serif font $(\mathsf{v}_1, \mathsf{v}_2, \mathsf{v}_3)$. Defining a vector field $\mathbf{u} = \mathsf{u}_1\mathbf{d}_1 + \mathsf{u}_2\mathbf{d}_2 + \mathsf{u}_3\mathbf{d}_3$, the Darboux vector, the s-evolution of the orthonormal basis $(\mathbf{d}_1, \mathbf{d}_2, \mathbf{d}_3)$ is given by the differential system:

$$\mathbf{d}_j' = \lambda\,\mathbf{u}(s) \times \mathbf{d}_j(s)\,, \quad j = 1, 2, 3. \tag{6}$$

Then soving the O.D.E $\mathbf{r}' = \mathbf{d}_3$ we can construct $\mathbf{r}$ and hence ribbon and tube structures using (4). The system (6) is linear and assuming the functions u_j are continuous its solution exists and is unique up to a rotation and translation given by the initial conditions (see e.g. [5]). In Section 4 we consider curves for which the functions u_j have a finite number of discontinuities, in this case a unique continous $\mathbf{v}$ (given some initial conditions) can be constructed by matching boundary conditions at the discontinuities.

2.2 Net winding/linking, Twist, and Writhe

2.3 The Net-Winding

Consider two curves $\mathbf{r}$ and $\mathbf{v}$ bound between two planes such as in Figure 3(a) and (c), they may be closed or open. Without loss of generality we will assume these planes have $\hat{\mathbf{z}}$ as normal. We parameterise the curves by their z co-ordinate and define the vector $\mathbf{u}(z) = \mathbf{v}(z) - \mathbf{r}(z)$ which lies in a particular z-plane, along with the associated angle $\Theta(z)$ it makes with the x-axis, see Figure 3(b). In general curves $\mathbf{r}$ and $\mathbf{v}$ might turn back on themselves in the z-direction ($\mathrm{d}r_z/\mathrm{d}s = 0$, $\mathrm{d}^2r_z/\mathrm{d}s^2 \neq 0$), we call these points *turning points*. Say the

curve $\mathbf{r}$ (respectively $\mathbf{v}$) has n (resp. m) such turning points then there are $n+1$ sections $\mathbf{r}_i\,, i=1,\dots n+1$ (resp. $m+1$ sections $\mathbf{v}_j\,, j=1,\dots m+1$), then each pair of sections shares a (possibly empty) mutual range of z values $z\in[z_{ij}^{\min}, z_{ij}^{\max}]$. The *net winding* $\mathcal{L}_p(\mathbf{r},\mathbf{v})$ is given by the formula

$$\mathcal{L}_p(\mathbf{r},\mathbf{v}) = \sum_{i=1}^{n+1}\sum_{j=1}^{m+1}\frac{\sigma_i\sigma_j}{2\pi}\int_{z_{ij}^{\min}}^{z_{ij}^{\max}}\frac{\mathrm{d}\Theta_{ij}}{\mathrm{d}z}\,\mathrm{d}z = \frac{\Theta_{(n+1)(m+1)}-\Theta_{11}}{2\pi} + \sum_{i=1}^{n+1}\sum_{j=1}^{m+1}\sigma_i\sigma_j\,n_{ij} \tag{7}$$

where $\sigma_i=+1$ if the section is moving upward, and $\sigma_i=-1$ if the section is moving downward, $\Theta_{(n+1)(m+1)}$ the end angle on the upper bounding plane, Θ_{11} the angle on the lower bounding plane and n_{ij} the integer number of windings between sections $\mathbf{r}_i$ and $\mathbf{v}_j$. The angles Θ_{11} and $\Theta_{(n+1)(m+1)}$ are formally zero if the curves are closed. In [12] the following properties of $\mathcal{L}_p(\mathbf{r},\mathbf{v})$ were demonstrated

- $\mathcal{L}_p$ is invariant during continuous deformations of the two curves provided (*i*) the curves don't cross (isotopies), (*ii*) the end angles Θ_{11} and $\Theta_{(n+1)(m+1)}$ remain fixed, and (*iii*) the curves remain between the bounding planes $r_z(s_{\min}) = const$ and $r_z(s_{\max}) = const$.
- If $\mathbf{r}$ and $\mathbf{v}$ pass through each other $\mathcal{L}_p$ jumps by ± 1.
- For closed curves $\mathcal{L}_p(\mathbf{r},\mathbf{v}) = \mathcal{L}(\mathbf{r},\mathbf{v})$, where $\mathcal{L}$ is the well known Linking integer.

So the net winding extends the notion of linking to include open curves bound between two planes. We should add that the boundary planes can move, as for example a ribbon structure of fixed length which is compressed leading to its ends to move toward each other (see e.g. Figure 3(a)-(c)).

The Twist

The twist $\mathcal{T}$ is the total rotation of $\mathbf{d}_1$ about $\mathbf{d}_3$,

$$\mathcal{T}(\mathbf{r},\mathbf{d}_1) = \frac{1}{2\pi}\int_{s_{\min}}^{s_{\max}}\mathbf{d}_3\cdot(\mathbf{d}_1\times\mathbf{d}_1')\,\mathrm{d}s = \frac{1}{2\pi}\int_{s_{\min}}^{s_{\max}}\mathtt{u}_3\,\mathrm{d}s. \tag{8}$$

This definition is independent of the choice of angle ξ used to obtain the ribbon from the tube [12]. $\mathcal{T}$ changes continuously under continuous deformations of $\mathbf{r}$. The twist rate $\mathrm{d}\mathcal{T}/\mathrm{d}s$ is a variable in elastic rod theories [7, 4] and polymer models [11, 21, 14, 19]. A key result we use later is as follows: for any twice-differentiable curve $\mathbf{r}$ we can define a ribbon $\mathbf{v}(s)=\mathbf{r}(s)+\epsilon\,\mathbf{d}_1(s)$ for which $\mathcal{T}'=0$ (see [13]). The twist, as a net rotation, is also well defined for vector fields $\mathbf{d}_1$ which are only piecewise differentiable with a finite set of discontinuities. In this case (8) is the sum of a finite number of integrals split at the discontinuous points.

2.4 The Polar Writhe

The polar writhe $\mathcal{W}_p$ is the sum of local and non-local components

$$\mathcal{W}_p(\mathbf{r}) = \mathcal{W}_{pl}(\mathbf{r}) + \mathcal{W}_{pnl}(\mathbf{r}). \tag{9}$$

Using its turning points we decompose $\mathbf{r}$ into $n+1$ sections $\mathbf{r}_i\,, i=1,\dots n+1$. The local component is given by the arc-length integral

$$\mathcal{W}_{pl}(\mathbf{r}) = \sum_{i=1}^{n+1}\frac{\sigma_i}{2\pi}\int_{s_i^{\min}}^{s_i^{\max}}\frac{\hat{\mathbf{z}}\cdot\mathbf{d}_3\times\mathbf{d}_3'}{1+||\hat{\mathbf{z}}\cdot\mathbf{d}_3||}\,\mathrm{d}s. \tag{10}$$

The non local contribution can be defined in a similar fashion to the net-winding. We define $\mathcal{W}_{pnl}$ to be the winding of all angles Θ_{ij} made by the vector field $\mathbf{r}_{ij}=\mathbf{r}_j-\mathbf{r}_i$ of each pair of sections (double counted), i.e.

$$\mathcal{W}_{pnl}(\mathbf{r}) = \sum_{\substack{i=1\\ i\neq j}}^{n+1}\sum_{j=1}^{n+1}\frac{\sigma_i\sigma_j}{2\pi}\int_{z_{ij}^{\min}}^{z_{ij}^{\max}}\frac{\mathrm{d}\Theta_{ij}}{\mathrm{d}z}\mathrm{d}z. \tag{11}$$

An example of such a calculation is shown in Figure 4. It was demonstrated in [12] that $\mathcal{W}_p$ has the following properties

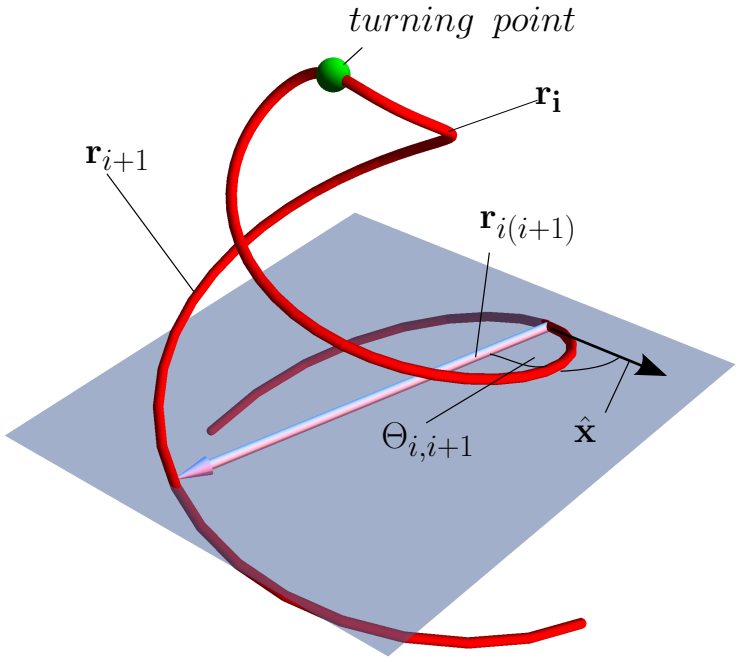

Figure 4: An example of a curve which has non-local polar writhing $\mathcal{W}_{pnl}$. The curve is split at its i^{th} turning point into sections $\mathbf{r}_i$ and $\mathbf{r}_{i+1}$. We see the vector $\mathbf{r}_{i(i+1)}$ whose winding contributes to $\mathcal{W}_{pnl}$.

- $\mathcal{W}_p$ changes continuously during isotopic deformations.
- If $\mathbf{r}$ self-crosses, it jumps by ± 2.
- For closed curves $\mathcal{W}_p(\mathbf{r}) = \mathcal{W}(\mathbf{r})$, where $\mathcal{W}$ is the writhing number (see *e.g.* [2]).

Finally in [12] it was shown that the above three quantities are linked by the following formila

$$\mathcal{L}_p(\mathbf{r}, \mathbf{d}_1) = \mathcal{T}(\mathbf{r}, \mathbf{d}_1) + \mathcal{W}_p(\mathbf{r}). \tag{12}$$

This was first demonstrated for closed curves by Călugăreanu [16, 17] and then demonstrated in a concise fashion by Pohl [39] (again for closed ribbons only). If the ribbon is significantly narrow the crossing of $\mathbf{r}$ with itself will essentially be equivalent to $\mathbf{v}$ crossing itself and discontinuous changes in $\mathcal{W}_p$ will coincide with that of $\mathcal{L}_p$. With this assumption we can use the writhe $\mathcal{W}_p$ to detect changes in topology of the ribbon. It is this context in which the Călugăreanu theorem is used in thin elastic rod and polymer studies, *e.g.* [21, 14, 43, 34, 6, 38, 19] amongst many. The decomposition (12) has also been used to study the changing morphology of coronal flux tubes [18, 27, 41, 49].

2.4.1 The local writhe for piecewise differentiable ribbons

As with the twist, the local polar writhe $\mathcal{W}_{pl}$ is also well-defined for curves whose tangent vector $\mathbf{d}_3$ is only piecewise differentiable. This is not explicitly stated in [12] where $\mathcal{W}_{pl}$ is defined as the difference $\mathcal{L}_p - \mathcal{T}$ of a ribbon $(\mathbf{r}, \mathbf{d}_1)$[a]. Since both $\mathcal{L}_p$ and $\mathcal{T}_p$ are well defined in such cases, we can construct a definition of $\mathcal{W}_{pl}$ which is also well defined. Consider a curve with **no** turning points for which the vector field $\mathbf{d}_1$ is only piecewise differentiable. The integrals for $\mathcal{L}$ and $\mathcal{T}$ on a domain $s \in [s_{\min}, s_{\max}]$ are split by the finite number l of discontinuous points s_i of the functions $\mathbf{u}_i$ defining $\mathbf{d}_1$. From [12] each difference $\mathcal{L}_p - \mathcal{T}$ on the domain $s \in [s_i, s_{i+1}]$ is given by the expression

$$\mathcal{W}_{pl}(\mathbf{r}, s_i, s_{i+1}) = \frac{\sigma_i}{2\pi} \int_{s_i}^{s_{i+1}} \frac{\hat{\mathbf{z}} \cdot \mathbf{d}_3 \times \mathbf{d}_3'}{1 + ||\hat{\mathbf{z}} \cdot \mathbf{d}_3||} \mathrm{d}s. \tag{13}$$

[a]Its value is then shown to only depend on $\mathbf{r}$.

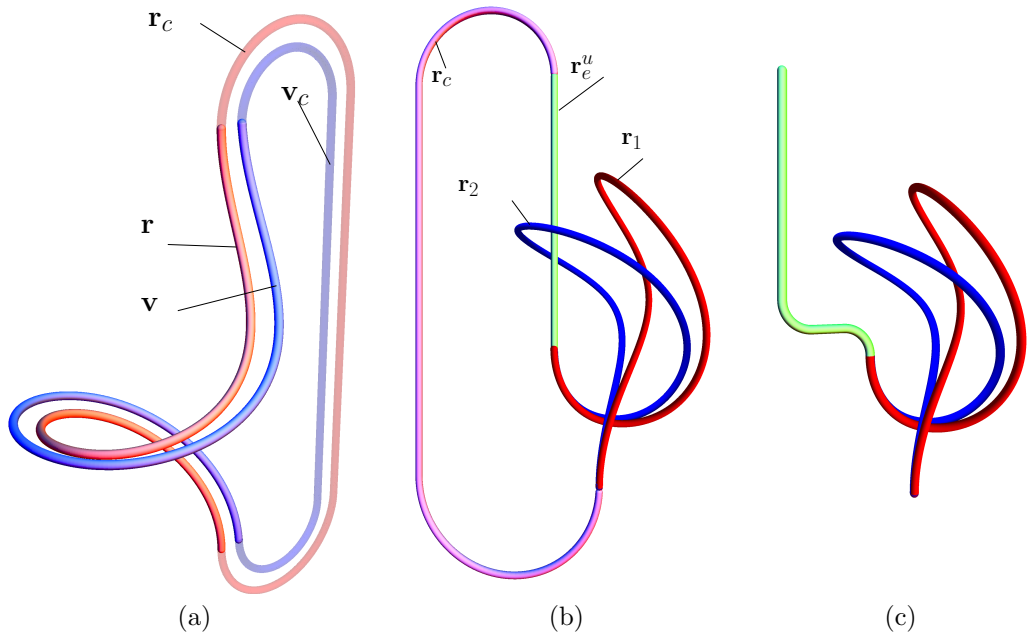

Figure 5: (a) depicts a planar stadium closure curve typically used in a number of studies, the opaque sections $\mathbf{r}_c$ and $\mathbf{v}_c$ are the closure of the initial ribbon. (b) depicts pair of curves from the knotting type deformation path detailed in Section 6.3. We show an extension $\mathbf{r}_e^u$ which is crossed during an end-restricted isotopy path from curve $\mathbf{r}_1$ to curve $\mathbf{r}_2$. Also shown is a closure $\mathbf{r}_c$ which is the union of the extension and a stadium-type curve. (c) shows an alternative (planar) extension which is not crossed during the deformation.

and the total $\mathcal{W}_{pl}$ value is

$$\mathcal{W}_{pl}(\mathbf{r}) = \mathcal{W}_{pl}(\mathbf{r}, s_{\min}, s_1) + \sum_{i=1}^{l} \mathcal{W}_{pl}(\mathbf{r}, s_i, s_{i+1}) + \mathcal{W}_{pl}(\mathbf{r}, s_l, s_{\max}). \tag{14}$$

For curves which have n turning points we must make this decomposition for each component of the sum (10).

2.5 Double Integral Formula

For closed curves the quantity $\mathcal{W}$ (equal $\mathcal{W}_p$) can be calculated using the following double integral expression

$$\mathcal{W}(\mathbf{r}) = \frac{1}{4\pi} \oint_{\mathbf{r}} \oint_{\mathbf{v}} \frac{[\mathbf{r}'(s) \times \mathbf{r}'(s^\star)] \cdot [\mathbf{r}(s) - \mathbf{r}(s^\star)]}{||\mathbf{r}(s) - \mathbf{r}(s^\star)||^3} \, \mathrm{d}s \, \mathrm{d}s^\star \tag{15}$$

[2]. If $\mathbf{r}$ is not closed then this double integral differs from $\mathcal{W}_p$, however, it was shown in [12] that we can always form a twice-differentiable composite curve $\mathbf{r} \cup \mathbf{r}_c$, where $\mathbf{r}_c$ joins the $\mathbf{r}(s_{min})$ to $\mathbf{r}(s_{max})$, for which $\mathcal{W}(\mathbf{r}+\mathbf{r}_c) = \mathcal{W}_p(\mathbf{r})$. Creating a composite curve $\mathbf{r} \cup \mathbf{r}_c$ is the procedure used in [43, 46, 51] to apply topological constraints to open elastic rods. There are a number of existing algorithms used to calculate (15) which we use to as a comparison to demonstrate the efficiency of the polar writhe formulation in assessing open ribbon topology.

3 Over the Top Curves

As it stands (12) is not applicable to curves for whom a section crosses the bounding planes, see for example the curves shown in Figure 5. More precisely if $r_z(s_{\max}) > r_z(s_{\min})$ and there is some subset or union of

subsets of $[s_{\min}, s_{\max}]$ for which either $r_z(s) > r_z(s_{\max})$ or $r_z(s) < r_z(s_{\min})$, then $\mathcal{L}_p(\mathbf{r}, \mathbf{d}_1)$ is no longer an invariant (an equivalent statement in the case where $r_z(s_{\max}) < r_z(s_{\min})$ should be obvious). The main goal of the present work is to extend the definition of $\mathcal{W}_p$ so that the sum $\mathcal{W}_p + \mathcal{T}$ is conserved in such cases.

Of course the issue of allowing such deformations is that they allow for the loss of total winding through the belt trick or knotting, both isotopies. One way of detecting such changes is to append a closure to the curve, as in Figure 5(a). We create a closed composite curve $\mathbf{r} \cup \mathbf{r}_c$ and differentiable periodic vector field $\mathbf{v} \cup \mathbf{v}_c$. This is the procedure followed in [3, 43, 46, 51]. The ribbon had to be closed in these studies as the authors used the Gauss linking integral $\mathcal{L}$, not the more general net-winding $\mathcal{L}_p$. With this closure we can track continuous conversion of writhing into twisting through the difference $\mathcal{L} - \mathcal{W}$. Any deformations such as the knotting deformation shown in Figure 2 will guarantee that this closure is crossed causing both the linking and writhing to jump by the same integer value. This will also allow for the tracking of changes in the topological nature of the winding of the curve, which the belt trick provides, through the ± 2 change in linking. This would lead to the correct evaluation of the final linking of the belt-trick deformation. However, one must take care in defining the closure. A poorly chosen closure could add linking to the composite calculation $\mathcal{L}(\mathbf{r} \cup \mathbf{r}_c, \mathbf{d}_1 \cup \mathbf{d}_{1c})$ by knotting the curve further. We can always ensure this pitfall is avoided by applying a sufficiently large stadium closure to avoid knotting with the original curve any further, as discussed in [43]. However, in order to accurately evaluate the writhing of such curves one must take the contribution of the closure into account accurately, leading to an excessive computational cost and difficulty in developing a general code to construct an appropriate closure for any given curve. Also if the end tangents are not aligned a general prescription for this closure procedure could prove difficult.

By comparison, for the net winding it is sufficient to simply extend the curve upwards or downwards such that the new extended curve is completely contained between its end planes, as for the composite curves $\mathbf{r}_1 \cup \mathbf{r}_e^u$ or $\mathbf{r}_2 \cup \mathbf{r}_e^u$ in Figure 5(b) for example. We show in Section 4 that it is always sufficient to extend the curve straight up (or down), from the original curve's end points, along $\hat{\mathbf{z}}$ (*resp.* -$\hat{\mathbf{z}}$). This would not produce a differentiable curve when the end tangents do not align, but we show there always exists a differentiable pair of curves, $\mathbf{r}_e^u$ (up) and $\mathbf{r}_e^d$ (down), which differ form straight line extension by an arbitrarily small amount (Theorem 1 of Section 4) and whose extended $\mathcal{W}_p(\mathbf{r}_e^d \cup \mathbf{r} \cup \mathbf{r}_e^u)$ measure is equal to the straight closure case. The details of this extension are somewhat fiddly so we relegate them to Section 4. Before this we give an explicit definition of the quantity $\mathcal{W}_p^\star$, which does not require details of the extension $\mathbf{r}_e$. We shall also demonstrate its utility through example calculations in Section 6.

3.1 The Extended Polar Writhe Measure $\mathcal{W}_p^\star$

In the proof of Theorem 1 in Section 4 we demonstrate that the extensions $\mathbf{r}_e^u$ and $\mathbf{r}_e^d$ can always be constructed such that $\mathcal{W}_{pl}(\mathbf{r}_e^d \cup \mathbf{r} \cup \mathbf{r}_e^u) = \mathcal{W}_{pl}(\mathbf{r})$: the local component only depends on the original curve's geometry. For the non-local component $\mathcal{W}_{pnl}(\mathbf{r}_e^d \cup \mathbf{r} \cup \mathbf{r}_e^u) \neq \mathcal{W}_{pnl}(\mathbf{r})$ and its definition requires a little alteration.

We assume here that the curve $\mathbf{r}$ has upward pointing tangents at both extremities: $\mathbf{d}_{3z}(s_{\min}, s_{\max}) > 0$. As before there are n turning points along $\mathbf{r}$ and hence $n+1$ sections. In a section i, if a point is such that $\mathbf{r}_i(s_i^+)$ has its z coordinate equal to $r_z(s_{max})$, we record the angle Θ_i^+ made by the vector $\mathbf{r}_i(s_i^+) - \mathbf{r}(s_{\max})$ and the x-axis. Otherwise Θ_i^+ is set to zero. Conversely if a point is such that $\mathbf{r}_i(s_i^-)$ has its z coordinate equal to $r_z(s_{min})$, we record the angle Θ_i^- made by the vector $\mathbf{r}_i(s_i^-) - \mathbf{r}(s_{\min})$ and the x-axis. Otherwise Θ_i^- is set to zero. The non local polar writhe $\mathcal{W}_{pnl}(\mathbf{r})$ can then be written in terms of the following quantities [12, 40]:

1. at each turning point k, the angle ϕ_k ($\in [0, 2\pi)$) made by the tangent vector $\mathbf{d}_3$ with the x-axis
2. n_{ij}, the signed number of full turns made by Θ_{ij} for sections i and j of the curve
3. the angles Θ_i^+ and Θ_i^- made by the curve's end points and sections of the curve sharing a mutual z value.

and we have

$$\mathcal{W}_{pnl}(\mathbf{r}) = \frac{1}{2\pi}\left[\sum_{k=1}^{n} 2\,\eta_k\,\phi_k + \sum_{\substack{i=1\\ i\neq j}}^{n+1}\sum_{j=1}^{n+1}\sigma_i\sigma_j n_{ij} + \sum_{i=1}^{n+1}(-1)^{i+1}\,\Theta_i^{+} + (-1)^{i}\,\Theta_i^{-}\right] \tag{16}$$

with $\eta_k = +1$ (respectively $\eta_k = -1$) if the k^{th} turning point is a local minimum (respectively maximum) in z. Crucially the sum $\mathcal{W}_p(\mathbf{r}) + \mathcal{T}(\mathbf{r}, \mathbf{d}_1)$ is not generally invariant when there are end angles Θ_i^{+} or Θ_i^{-}, we demonstrate this numerically in section (6). The extensions $\mathbf{r}_e^d$ and $\mathbf{r}_e^u$ will ensure that there are no end angles Θ^{+} or Θ^{-} made by the extended curve $\mathbf{r}_e^d \cup \mathbf{r} \cup \mathbf{r}_e^u$ with itself. Also $\mathbf{r}_e^d$ and $\mathbf{r}_e^u$ are straight lines with no turning points, so the turning angle sum will not change under this extension, nor will the extensions have any full windings with themselves. With this we can define a new quantity $\mathcal{W}_p^{\star}(\mathbf{r})$

$$\mathcal{W}_p^{\star}(\mathbf{r}) = \mathcal{W}_{pl}(\mathbf{r}) + \frac{1}{2\pi}\left[\sum_{k=1}^{n} 2\,\eta_k\,\phi_k + \sum_{\substack{i=1\\ i\neq j}}^{n+1}\sum_{j=1}^{n+1}\sigma_i\sigma_j n_{ij}\right] \tag{17}$$

The only contribution to the quantity $\mathcal{W}_p^{\star}$ from the extensions arises from integer winding of the union $\mathbf{r}_{n+1} \cup \mathbf{r}_e^u$ and any other section of the curve $\mathbf{r}_i$, $i \neq n+1$ and similarly union $\mathbf{r}_e^d \cup \mathbf{r}_1$ with any other section $\mathbf{r}_i$, $i \neq 1$.

Finally in Theorem 2 it is demonstrated that we can always define a ribbon structure $\mathbf{v}_e^u = \mathbf{r}_e^u + \epsilon\,\mathbf{d}_{1e}^u$ and $\mathbf{v}_e^d = \mathbf{r}_e^d + \epsilon\,\mathbf{d}_{1e}^d$, for which $\mathcal{T}(\mathbf{r}_e^u, \mathbf{v}_e^u) = 0$ and $\mathcal{T}(\mathbf{r}_e^d, \mathbf{v}_e^d) = 0$, so the quantity

$$\mathcal{W}_p^{\star}(\mathbf{r}) + \mathcal{T}(\mathbf{r}, \mathbf{d}_1) \tag{18}$$

is equivalent to the sum

$$\mathcal{W}_p(\mathbf{r}_e^d \cup \mathbf{r} \cup \mathbf{r}_e^u) + \mathcal{T}(\mathbf{r}_e^d \cup \mathbf{r} \cup \mathbf{r}_e^u, \mathbf{d}_{1e}^d \cup \mathbf{d}_1 \cup \mathbf{d}_{1e}^u) \tag{19}$$

which is a pair of curves bound between two planes and hence invariant in any non-self-intersecting end-isotopy. The results of [12] show this extension can always be extended to a closed curve $\mathbf{r} \cup \mathbf{r}_c$ for which (18) is equivalent to

$$\mathcal{W}(\mathbf{r} \cup \mathbf{r}_c) + \mathcal{T}(\mathbf{r} \cup \mathbf{r}_c, \mathbf{d}_1 \cup \mathbf{d}_{1c}). \tag{20}$$

(There $\mathbf{r}_c$ would comprise our extensions plus a classical closure curve as in Figure 5(a)). We demonstrate this numerically in Section 6.

3.2 A Note on End-Angles and the Choice of Extension

A key difference between the writhing measures $\mathcal{W}_p(\mathbf{r})$ and $\mathcal{W}_p^{\star}(\mathbf{r})$ is the end-angles made by sections of $\mathbf{r}$ and the end points $\mathbf{r}(s_{\min})$ and $\mathbf{r}(s_{\max})$, if they exist. Since the curve $\mathbf{r}$ is continuous, it can only rise above(below) the end-planes as one or several looped section(s), see for example Figure 6. Each looped section leads to two such end angles $\Theta_i^{+/-}$ and $\Theta_{i+1}^{+/-}$, each prefaced with an opposing sign due to the functions σ_i σ_{i+1} (as the curve sections are moving up and down). Thus the sum of these angles (Φ) will be (up to a sign) the angle made by the vectors joining the two looped footpoints and the end point (Figure 6(b)). Now, consider a knotting or belt-trick type deformation, for which this looped section passes over the top of the curves ends, Φ starts at 0 and gradually increases to 2π as the loop passes over the end point (Figure 6(b)). When the loop passes back below the end plane the measure $\mathcal{W}_p$ there would have registered this integer change in angle, which is counted twice in the sum $\mathcal{W}_p$. The extensions $\mathbf{r}_e^d$ and $\mathbf{r}_e^u$ ensure that the quantity $\mathcal{W}_p^{\star}$ registers this integer change half way through this deformation when the curve crosses the extension (as would have occurred in the isotopy joining the two curves in Figure 5(a)).

Of course we could have chosen alternative extensions which avoid this crossing as shown in Figure 5(c). However, as demonstrated in Figure 6(a) any such choice of closure would eventually have been crossed when the 2π change in angle occurs. Since open curves are never really truly knotted (the sense of knotting is given by the closure) there will always be some sense of ambiguity in the choice of closure/extension. Our

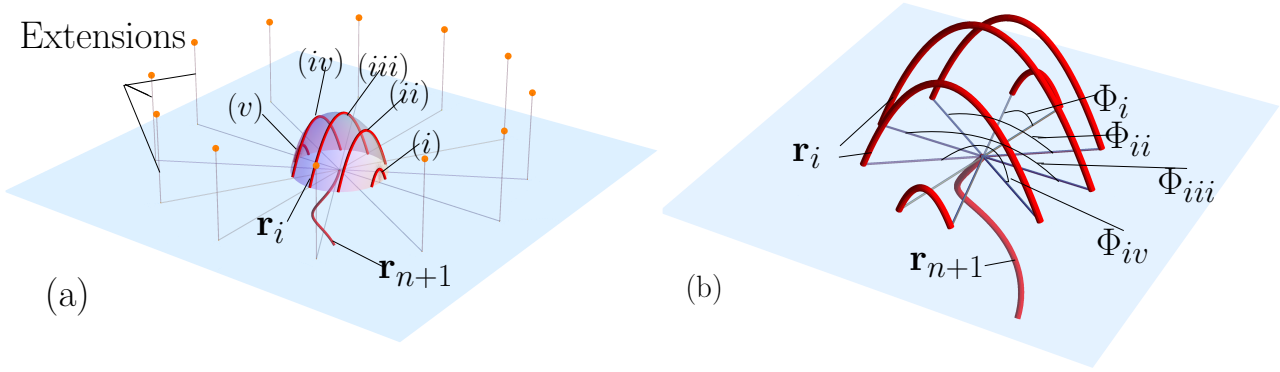

Figure 6: Figures depicting a looped section of curve $\mathbf{r}_i$ deforming over the top of the end point attached to section $\mathbf{r}_{n+1}$. In (a) we see the envelope of points drawn out by the deforming path of the looped section, this isotopy path is represented by a set of curves (i)-(v) . Also shown are a subset of the possible extensions one could create to make the sum $\mathcal{W}_p + \mathcal{T}$ invariant, each of which would be crossed at some point during this isotopy path. In (b) we see the set of angles $\Phi_i, \Phi_{ii}, \Phi_{iii}$ and Φ_{iv} (Φ_v is not shown for clarity) which are made by the vectors joining the points where the looped section $\mathbf{r}_i$ intersects the plane $z = r_z(s_{\max})$. As the section passes over the end point the angle Φ gradually increases to 2π.

extension gives the sum $\mathcal{W}_p + \mathcal{T}$ which would be obtained by pulling the end points of the curve in opposing directions ($\hat{\mathbf{z}}$ and -$\hat{\mathbf{z}}$) such that, when treated as a narrow incompressible and unstretchable tube) the end to end distance of the points will attain its maximum possible value, this will be either a tightened knot or a straight ribbon. This "pulled tight" configuration is independent of the choice of closure. We believe this is a sensible and practical choice for separating the space of possible ribbon configurations into a set of domains in which the sum $\mathcal{W}_p + \mathcal{T}$ is conserved.

Further, one of the main features of twist-writhe decomposition is that the changing writhe tells us the topologically permissible change in internal twisting due to the changing shape of the tube. This change is continuous under isotopy and determined by the sum $\mathcal{W}_{pl} + \mathcal{T}$, a closure independent sum. It is the nonlocal part W_{pnl} which changes discontinuously as the net winding $\mathcal{L}_p$ does.

4 Constructing the Extension

In what follows we demonstrate that we can always define a curve $\mathbf{r}_e$ which extends the curve $\mathbf{r}$ from its end points such that the maximum and minimum r_z values of the original curve $\mathbf{r}$ are contained within the $z = const$ planes of the extension's end points. We show this extension can always be chosen have no local polar writhing $\mathcal{W}_{pl}(\mathbf{r}_e) = 0$ and that can be made arbitrarily close to a straight line curve section extending along $\hat{\mathbf{z}}$ (or $-\hat{\mathbf{z}}$) from $\mathbf{r}(s_{\max})$ (or $\mathbf{r}(s_{\min})$), see *e.g.* Figure 5(b).

One way to ensure that $\mathcal{W}_{pl}(\mathbf{r}) = 0$ for any curve $\mathbf{r}$ is to require that

$$\hat{\mathbf{z}} \cdot \mathbf{d}_3 \times \mathbf{d}_3' = 0. \tag{21}$$

for the whole curve. This is clearly true of curves with constant tangent vectors (straight lines). It is also easy to see it is true of sections of curve with the following general form

$$\mathbf{r}(t) = a\left(\cos(b)\cos(ct+d), \sin(b)\cos(ct+d), \sin(ct+d)\right), \tag{22}$$

with (a, b, c, d) arbitrary real constants. By constructing our extension $\mathbf{r}_e$ from a combination of circular section and a straight line we ensure it will have no local writhing. Our extension curve $\mathbf{r}_e$, it is the union of the following curve sections

1. A circular section $\mathbf{r}^r$ which re-orients the curve's end tangent $\mathbf{d}(s_{\max})$ (or $-\mathbf{d}(s_{\min})$) to point along $\hat{\mathbf{z}}$ (*resp.* -$\hat{\mathbf{z}}$).

2. A straight line joining the end of $\mathbf{r}^r$ to a point with a z co-ordinate above (below) the maximum (minimum) z value of the original curve.

4.1 Explicit Form

We define the circular section as a curve $[0,1] : \mathbf{r}^r(t) \to \mathbb{E}^3$ which takes the form

$$\mathbf{r}^r(t) = \mathbf{r}^{ri} + a\left[\frac{\epsilon^r}{\theta^r}\left(\cos\phi^r, \sin\phi^r, -\sin\theta^{rc}\right) - \frac{\epsilon^r}{\mathrm{d}\theta^r/\mathrm{d}t}\left(\cos\phi^r\cos\theta^r(t), \sin\phi^r\cos\theta^r(t), -\sin\theta^r(t)\right)\right], \tag{23}$$

$$\mathbf{r}^{ri} = \begin{cases} \mathbf{r}(s_{\max}), & \text{if } r_z^{ce} > r_z(s_{\max}) \\ \mathbf{r}(s_{\min}), & \text{if } r_z^{ce} < r_z(s_{\min}) \end{cases}, \quad \theta^r(t) = \begin{cases} \theta^{rc}(1-t), & \text{if } r_z^{ce} > r_z(s_{\max}) \\ \theta^{rc} + t(\pi - \theta^{rc}), & \text{if } r_z^{ce} < r_z(s_{\min}) \end{cases},$$

$$a = \begin{cases} -1, & \text{if } r_z^{ce} > r_z(s_{\max}) \\ 1, & \text{if } r_z^{ce} < r_z(s_{\min}) \end{cases}$$

$$\theta^{rc} = \begin{cases} \arccos(\hat{\mathbf{z}}\cdot\mathbf{d}_3(s_{\max})), & \text{if } r_z^{ce} > r_z(s_{\max}) \\ \arccos(-\hat{\mathbf{z}}\cdot\mathbf{d}_3(s_{\max})), & \text{if } r_z^{ce} < r_z(s_{\min}) \end{cases}, \quad \phi^r = \begin{cases} \arctan\left(\frac{\hat{\mathbf{y}}\cdot\mathbf{d}_3(s_{\max})}{\hat{\mathbf{x}}\cdot\mathbf{d}_3(s_{\max})}\right), & \text{if } r_z^{ce} > r_z(s_{\max}) \\ \arctan\left(\frac{\hat{\mathbf{y}}\cdot\mathbf{d}_3(s_{\min})}{\hat{\mathbf{x}}\cdot\mathbf{d}_3(s_{\min})}\right), & \text{if } r_z^{ce} < r_z(s_{\min}) \end{cases}.$$

The constant ϵ^r determines the velocity of the parametrisation ($\epsilon^r = 1$ would make t the arclength parameter of $\mathbf{r}^r$), it is also the total arclength of the curve as

$$\int_0^1 \sqrt{\frac{\mathrm{d}\mathbf{r}}{\mathrm{d}t}\cdot\frac{\mathrm{d}\mathbf{r}}{\mathrm{d}t}} = \epsilon^r.$$

We are now ready for our first theorem.

Theorem 1 *Given any curve $\mathbf{r}$ whose end tangents satisfy $d_{3z}(s_{\min}) > 0$ and $d_{3z}(s_{\max}) > 0$, with a point s_o satisfying $r_z(s_o) > r_z(s_{\max})$ (respectively $r_z(s_o) < r_z(s_{\min})$) we can construct a differentiable curve $\mathbf{r}_e \in [s_{\max}, M]$ (resp $\mathbf{r}_e \in [M, s_{\min}]$) and a composite curve $\mathbf{r} \cup \mathbf{r}_e$ (resp. $\mathbf{r}_e \cup \mathbf{r}$). The end point $\mathbf{r}_e(M)$ of this composite curve has the maximum (resp. minimum) $r_z(s)$ value on $s \in [s_{\min}, s_{\max}]$. Additionally we can always choose this curve such that $\mathcal{W}_{pl}(\mathbf{r}_e) = 0$.*

Proof of Theorem 1 If $r_z(s_o) > r_z(s_{\max})$, the closure $\mathbf{r}_e(t^e)$, with $t^e \in [s_{\max}, M]$, is

$$\mathbf{r}_e(t^e) = \begin{cases} \mathbf{r}^r\left(t^e/\epsilon^r\right), & \text{if } t^e \in [s_{\max}, \epsilon^r], \\ \mathbf{r}^r(1) + (0,0, r_z(s_o) + \beta - r_z^r(1))\frac{t-\epsilon^r}{M-\epsilon^r} & \text{if } t^e \in [\epsilon^r, M]. \end{cases} \tag{24}$$

with $\beta > 0$. If $r_z(s_o) > r_z(s_{\max})$ total the closure $\mathbf{r}_e(t^e),\ t^e \in [M, s_{\min}]$ is

$$\mathbf{r}_e(t^e) = \begin{cases} \mathbf{r}^r(1) + (0,0, r_z(s_o) - \beta - r_z^r(1))\frac{t-\epsilon^r}{M-\epsilon^r} & \text{if } t^e \in [M, \epsilon^r], \\ \mathbf{r}^r\left(1 - t^e/\epsilon^r\right), & \text{if } t^e \in [\epsilon^r, s_{\min}], \end{cases} \tag{25}$$

again with $\beta > 0$. The parameter β ensures $\mathbf{r}_e(M)$ has the maximum/minimum r_z value of the composite $\mathbf{r} \cup \mathbf{r}_e$ (*resp.* $\mathbf{r}_e \cup \mathbf{r}$).

Each individual section is infinitely differentiable but the whole curve $\mathbf{r}_e$ is only guaranteed to be once differentiable at $t = s_{\max}$ or $s_{\min}$ and $t = \epsilon^r$, thus the local polar writhe calculation is split into two separate integrals,

$$\mathcal{W}_{pl}(\mathbf{r}_e) = \mathcal{W}_{pl}(\mathbf{r}_e, 0, \epsilon^r) + \mathcal{W}_{pl}(\mathbf{r}_e, \epsilon^r, M). \tag{26}$$

We have already seen that the local writhe density $\frac{\partial \mathcal{W}_{pl}}{\partial t^e}$ of both circular and straight line curves is zero, thus $\frac{\partial \mathcal{W}_{pl}}{\partial t^e}$ vanishes on the whole domain $t^e \in [0, M]$ and hence $\mathcal{W}_{pl}(\mathbf{r}_e) = 0$ □

Next we show the ribbon $(\mathbf{r}, \mathbf{d}_1)$ can be extended with a ribbon section $(\mathbf{r}_e, \mathbf{d}_{1e})$ which has no additional twist. To do so we note that is shown in [13] that a ribbon for which $\mathcal{T}' = \mathsf{u}_3 = 0$ can be obtained by setting

$\mathsf{u}_2 = k_1$, $\mathsf{u}_1 = -k_2$ and $u_3 = 0$, where functions $k_1(s)$ and $k_2(s)$ can be obtained form the curve $\mathbf{r}$ in terms of its curvature κ and torsion τ through

$$k_1(\mathbf{r},s) = \kappa(\mathbf{r},s)\,\cos\psi(\mathbf{r},s)\,, \quad k_2(\mathbf{r},s) = \kappa(\mathbf{r},s)\,\sin\psi(\mathbf{r},s)\,, \quad \psi(\mathbf{r},s) = \psi_0 + \int_{s_{\min}}^{s} \tau(\mathbf{r},t)\,\mathrm{d}t \tag{27}$$
$$\kappa(\mathbf{r},s) = \frac{||\mathbf{r}'\times\mathbf{r}''||}{||\mathbf{r}'||^3}\,, \quad \tau(\mathbf{r},s) = \frac{(\mathbf{r}'\times\mathbf{r}'')\cdot\mathbf{r}'''}{||\mathbf{r}'\times\mathbf{r}''||^2}$$

with ψ_0 determined by the initial conditions. We are now ready for the theorem.

Theorem 2 *The extension $\mathbf{r}_e$ given by either (24) or (25) can be extended to a ribbon with a vector field $\mathbf{d}_{1e}$, such that $\mathbf{d}_{1e}(s_{\max}) = \mathbf{d}_1(s_{\max})$ (resp $\mathbf{d}_{1e}(s_{\min}) = \mathbf{d}_1(s_{\min})$) and $\mathcal{T}(\mathbf{r}^e, \mathbf{d}_{1e}) = 0$.*

Proof of Theorem 2 From the curve $\mathbf{r}_e$ we construct a twist-free framing using (27). For the straight curve section on $t^s \in (\epsilon^r, M]$ (*resp* $t^s \in [M, \epsilon^r)$) the second t^e derivative of $\mathbf{r}_e$ vanishes so $k_1 = k_2 = 0$. For both cases the curve section $\mathbf{r}^r$ has curvature

$$\kappa = \frac{\frac{\mathrm{d}\theta^r}{\mathrm{d}t}}{\epsilon^r}, \quad \tau = 0. \tag{28}$$

If $r_z(s_o) > r_z(s_{\max})$ we have $\tau(\mathbf{r}_e, t^e) = 0,\ \forall t^e \in [s_{\max}, M]$ and

$$\kappa(\mathbf{r}_e, t^e) = \begin{cases} \frac{\mathrm{d}\theta^r}{\mathrm{d}t}/\epsilon^r & \text{if } t^e \in (s_{\max}, \epsilon^r] \\ 0 & \text{if } \ t^e \in (\epsilon^r, M]. \end{cases} \tag{29}$$

If $r_z(s_o) < r_z(s_{\min})$ we have $\tau(\mathbf{r}_e, t^e) = 0,\ \forall t^e \in [M, s_{\min}]$ and

$$\kappa(\mathbf{r}_e, t^e) = \begin{cases} 0 & \text{if } \ t^e \in [M, \epsilon^r) \\ \frac{\mathrm{d}\theta^r}{\mathrm{d}t}/\epsilon^r & \text{if } t^e \in [\epsilon^r, s_{\min}) \end{cases} \tag{30}$$

Since the torsion τ is zero everywhere, we have $\theta(t) = \theta_0$, $\forall t^e$ giving $k_1(\mathbf{r}_e, t^e) = \kappa(\mathbf{r}_e, t^e)\cos\theta^0$ and $k_2(\mathbf{r}_e, t^e) = \kappa(\mathbf{r}_e, t^e)\sin\theta^0$. So we have piecewise continuous profiles for $k_1(\mathbf{r}_e, t)$ and $k_2(\mathbf{r}_e, t)$ and we can construct a twist-free frame $\{\mathbf{a}_{3e}(l), \mathbf{a}_{1e}(l), \mathbf{a}_{2e}(l)\}$ on $l \in [0, M - s_{max}]$ (*resp.* $l \in [0, M - s_{\min}]$) through (6) which exists and is unique up to its initial condition given by the value of θ_0. In the case $r_z(s_o) < z_{min}$ we would have to construct the frame from s_{min} to M, so the orientation of its tangent vector $\mathbf{a}_{3e}$ must oppose the vector $\mathbf{d}_3$ at $s_{\min}$. With this we choose θ_0 such that

$$\mathbf{a}_{3e}(0) = \begin{cases} \mathbf{d}_3(s_{\max}), & \text{, if } r_z(s_o) > z_{\max}, \\ -\mathbf{d}_3(s_{\min}) & \text{, if } r_z(s_o) < z_{\min}. \end{cases}, \quad \mathbf{a}_{1e}(0) = \begin{cases} \mathbf{d}_1(s_{\max}) & \text{, if } r_z(s_o) > z_{\max}, \\ \mathbf{d}_1(s_{\min}) & \text{, if } r_z(s_o) < z_{\min}. \end{cases},$$
$$\mathbf{a}_{2e}(0) = \begin{cases} \mathbf{d}_2(s_{\max}) & \text{, if } r_z(s_o) > z_{\max}, \\ -\mathbf{d}_2(s_{\min}) & \text{, if } r_z(s_o) < z_{\min}. \end{cases}$$

We have then defined a continuous vector field $\mathbf{a}_{1e}$ which can be extended to a continuous twist free-ribbon

$$\mathbf{d}_{1e}(t^e) = \mathbf{a}_{1e}(t^e - s_{\max}),$$
$$\mathbf{v}^e(t^e) = \mathbf{r}_e(t^e) + \mathbf{d}_{1e}(t^e).$$

with if $r_z(s_o) > z_{\max}$ and

$$\mathbf{d}_{1e}(t^e) = \mathbf{a}_{1e}(t^e - s_{\min}),$$
$$\mathbf{v}^e(t^e) = \mathbf{r}_e(t^e) + \mathbf{d}_{1e}(t^e).$$

if $r_z(s_o) < z_{\min}$, which satisfies the properties mentioned in the statement of the proof. □

4.2 The Parameter ϵ, Straight Extensions and Self-Crossings

We are free to choose the parameter ϵ, the size of the curved re-alignment section, to be as small as we like. This parameter dictates the final end point of the curve $\mathbf{r}_e$. If we focus on the case $r_z(s_o) > r_z(s_{\max})$ the x and y co-ordinates of $\mathbf{r}_e(M)$ are given by.

$$\left(\mathbf{r}_x(s_{\max}) + \frac{2\epsilon \sin^2\left(\frac{\theta}{2}\right)\cos(\phi)}{\theta}, \mathbf{r}_y(s_{\max}) + \frac{2\epsilon \sin^2\left(\frac{\theta}{2}\right)\sin(\phi)}{\theta}\right), \tag{31}$$

(note the limit $\theta \to 0$, the tangent vectors pointing along $\hat{\mathbf{z}}\,(-\hat{\mathbf{z}})$ are well defined). The vertical straight line used as an extension for defining $\mathcal{W}_p^\star(\mathbf{r})$ would be

$$\mathbf{r}_{\text{vertical}} = \mathbf{r}(s_{\max}) + (0, 0, r_z(s_o) + \beta - r_z(s_{\max}))\,. \tag{32}$$

In the limit $\epsilon \to 0$ the coordinates (31) approach the coordinates of the original curve at $s = s_{\max}$ and the measure

$$\int_{s_{\max}}^{M} ||\mathbf{r}_e - \mathbf{r}_{\text{vertical}}||\,\mathrm{d}t. \tag{33}$$

converges to zero. A similar argument applies to any extension for the case $r_z(s_o) < r_z(s_{\min})$. It is this limit which we assume for our definition of $\mathcal{W}_p^\star$.

Finally a subset of the possible curve configurations would intersect this closure. As ϵ is made arbitrarily small this means intersecting the straight line section. To avoid this we can simply add an (arbitrarily small circular section to the line in order to avoid self crossing. In practice this amounts to assigning an angle to a pair of points, the first one on the original curve $\mathbf{r}$ and the second one on the extension $\mathbf{r}_e^u$ (or $\mathbf{r}_e^d$), both of which are at the same point (with the straight closure). These points share the height: $r_z = z_{\text{cross}}$ and we simply assign to this angle the value of the previous angle at the next lowest height $z < z_{\text{cross}}$ (note that the algorithm works on discretized curves).

5 The Elastic Rod Model

We summarize here the elastic rod model we are using. Equilibrium configurations are computed and their topology is assessed. We use equilibrium solutions because they generate a rich variety of shapes, but also because they arise in polymer and mechanical engineering applications. The conservation of topology associated with the sum (18) is not limited to equilibrium rod structures. It is true of dynamic elastic rod structures and other non-elastic ribbon/tube models. This model simply affords a means by which the utility of the extended polar writhe measure $\mathcal{W}_p^\star$ can be demonstrated.

Kinematics

A configuration for the elastic rod is determined by the centerline $\mathbf{r}(s)$ together with a material vector $\mathbf{d}_1(s)$, see *e.g.* [7, 4] for more comprehensive exposition of thin rod theory. The deformation of the rod's centerline and material is tracked using the Darboux vector $\mathbf{u}$. In what follows the rod is inextensible and unshearable and hence the parameter s is the arclength in both undeformed and deformed states, i.e. $\lambda = ||\mathbf{r}'|| = 1$. The rod has length L and we set $s_{\min} = 0$ and $s_{\max} = L$.

Mechanics

In the case of no external load (such as gravity, electrostatics, contact, ...) the rod's mechanics are determined by the balance equations

$$\mathbf{n}' = 0, \quad \mathbf{m}' + \mathbf{r}' \times \mathbf{n} = 0. \tag{34}$$

where $\mathbf{n}$ and $\mathbf{m}$ are the internal resultant force and moment acting across the rod cross section $s = \text{const}$. To complete the equations we assume a linear constitutive law for the moment:

$$\mathbf{m} = K_1\,\mathsf{u}_1\,\mathbf{d_1} + K_2\,\mathsf{u}_2\,\mathbf{d_2} + K_3\,\mathsf{u}_3\,\mathbf{d_3} \tag{35}$$

where K_1, K_2 are the bending rigidities, and K_3 the twist rigidity. As the rod is considered inextensible and unshearable, no constitutive relation is given for the force $\mathbf{n}$. Equation (35) is used to write the unknowns u_j as functions of the components m_j. The complete set of equations is then given by (3), (6), and (34) for the six unknown vectors $\mathbf{r}$, $\mathbf{d}_j$, $\mathbf{n}$, and $\mathbf{m}$.

The Boundary Value Problem

In the following studies we pose and solve the following boundary value problem. At the $s = 0$ end of the rod we specify the position and material frame:

$$\mathbf{r}(0) = (0, 0, 0), \quad \mathbf{d}_1(0) = (1, 0, 0), \quad \mathbf{d}_2(0) = (0, 1, 0), \quad \mathbf{d}_3(0) = (0, 0, 1). \tag{36}$$

the force $\{\mathsf{n}_j(0)\}$ and moment $\{\mathsf{m}_j(0)\}$ components at $s = 0$ being six unknowns. At the other end $s = L$ of the rod we then need to provide six conditions. We chose to specify the position $\mathbf{r}(L)$ and three of the nine components of the basis $(\mathbf{d}_1, \mathbf{d}_2, \mathbf{d}_3)$, as orthonormality then constrains the remaining six components. A continuation begins with a first solution of the equilibrium equations. We then chose to free one condition among the six $s = L$ conditions and we are left with a one dimensional family of solutions.

6 Results

In what follows we compute the equilibrium shapes of an elastic rod strongly held at both extremities, that is the position and the tangent are prescribed at both ends. In Section 6.1 the tangents are parallel and aligned with the vector joining the two ends, in Section 6.2 the tangents are not parallel, and in Section 6.3 the tangents are parallel but not aligned with the vector joining the two ends. Encountered configurations include straight and twisted, buckled, or knotted configurations. In each case we discretize the shapes $\mathbf{r}(s)$ into N points and we calculate $\mathcal{W}_p(\mathbf{r})$, $\mathcal{W}_p^\star(\mathbf{r})$, and $\mathcal{W}(\mathbf{r} \cup \mathbf{r}_c)$, given by the double integral formula (15). We put additional discretization points along $\mathbf{r}_c(t)$ in the last case.

Algorithms

For Case 1 and 3, calculations are performed using Mathematica. The quantity $\mathcal{W}(\mathbf{r} \cup \mathbf{r}_c)$ is calculated using the algorithm given in [47], and the quantities $\mathcal{W}_p$ and $\mathcal{W}_p^\star$ are calculated using code the authors have written which is available, see supplementary material. For Case 2, calculations are performed with C++. The quantity $\mathcal{W}(\mathbf{r} \cup \mathbf{r}_c)$ is calculated using the same [47] algorithm and a second code due to Agarwal *et al* [1]. The second algorithm is, to the best of our knowledge, the quickest available for evaluating the quantity $\mathcal{W}$ for a closed curve. We make no comparison to the algorithm of [29] as it was shown to be significantly slower than the Agarwal *et al* code in [1]. The quantities $\mathcal{W}_p$ and $\mathcal{W}_p^\star$ are calculated using code the authors have written which is available, see supplementary material. In all three cases, calculations were performed on computers with typically 2 to 3 GHz Intel Core i5 CPUs. For our time plots we use $T_0 = 0.4$ second as time unit. This is the time needed to compute $\mathcal{W}_p$ with 1000 points for configuration A of Case 1, using Mathematica 8 (for comparison this time is 0.01 second if one uses the C++ code).

6.1 Case 1: Parallel Tangents, Aligned Ends

We consider a rod with rigidities $K_1 = 1.0$, $K_2 = 1.1$, and $K_3 = 1.2$ and of unit length, $L = 1$, with position and tangent prescribed at both ends [b]. Moreover the tangents are parallel and aligned with the vector joining the two ends. The $s = 0$ conditions are given by (36) and the six $s = L$ conditions are given by:

$$r_x(L) = 0, \quad r_y(L) = 0, \quad r_z(L) = (1 - \Delta)L, \quad d_{3x}(L) = 0, \quad d_{3y}(L) = 0, \quad \alpha_L = 0.3 \times 2\pi \tag{37}$$

[b] The choices $K_1 = 1$ and $L = 1$ imply that we use L as the length unit, K_1/L^2 as the force unit, and K_1/L as the moment unit throughout this study.

where α_L (with $0 \leq \alpha_L < 2\pi$) is the rotation angle of $\mathbf{d}_1(L)$ in the basis $(\hat{\mathbf{x}}, \hat{\mathbf{y}})$. We start with a straight configuration $r_z(L) = L$ that has $\mathcal{T} = 0.3$, $\mathcal{W}_p = 0$, and $\mathcal{L}_p = \mathcal{T}$. Building a stadium closure $\mathbf{r}_c$ we have $\mathcal{W}(\mathbf{r} \cup \mathbf{r}_c) = 0$ and $\mathcal{L}(\mathbf{r} \cup \mathbf{r}_c, \mathbf{d_1} \cup \mathbf{d}_{1c}) = \mathcal{T}(\mathbf{r})$. The six unknowns at $s = 0$ take the values $\{\mathsf{n}_1, \mathsf{n}_2, \mathsf{n}_3\} = \{0, 0, -169.05\}$ and $\{\mathsf{m}_1, \mathsf{m}_2, \mathsf{m}_3\} = \{0, 0, 2.262\}$. The third condition in (37) involves the end-shortening $\Delta = 1 - r_z(L)/L$ which is increased from $\Delta = 0$ (buckling) up to $\Delta = 0.95$.

In Figure 7(a) we see a plot of the tension $\mathsf{n}_3(0)$ as a function of the end-shortening Δ, with four points A, B, C, D corresponding to the configurations plotted in Figure 8. Figure 7(c) shows a plot of the quantities $\mathcal{W}(\mathbf{r} \cup \mathbf{r}_c)$, $\mathcal{W}_p^\star$, and $\mathcal{W}_p$ as a function of Δ. The first is computed with $N = 48$ along the curve and $N/4 = 12$ additional points in the closure, and the last two with $N = 200$. The first two curves, $\mathcal{W}(\mathbf{r} \cup \mathbf{r}_c)$ and $\mathcal{W}_p^\star$, are always very close to each other, only differing because of computations errors. The third curve, $\mathcal{W}_p$, is very close to the first two, except after $\Delta \simeq 0.875$ where it clearly departs from the first two. Moreover two jumps are clearly visible for the three curves, and Figure 7(d) presents a close-up of the region of interest. Slightly after configuration B the rod experiences a self-crossing which is associated with a writhe discontinuity of -2. Then slightly before configuration C the rod experiences a double self-crossing which is associated with a writhe discontinuity of -4. Finally at $\Delta \simeq 0.875$ the rod has a section that passes above the plane $z = r_z(L)$. Starting for this point, $\mathcal{W}_p$ no longer yields correct values, and we see its curve departing form the other two curves. In 7(e) and (f) we see the sum of the various writhe measures and the twist, this sum being constant except for the discontinuous jumps, and for the sum $\mathcal{W}_p(\mathbf{r}) + \mathcal{T}(\mathbf{r}, \mathbf{d}_1)$ on the set of curves for which $\mathcal{W}_p^\star \neq \mathcal{W}_p$.

If we now consider the quantities (18) and (20) and focus on their decimal parts to disregard the jumps, we see that they should remain constant due to the fixed rotation α_L. In other words the quantities

$$\mathcal{E}^\star = mod\Big(\mathcal{W}_p^\star(\mathbf{r}) + \mathcal{T}(\mathbf{r}, \mathbf{d}_1), 1\Big) - \alpha_L/(2\pi) \tag{38}$$

and

$$\mathcal{E} = mod\Big(\mathcal{W}(\mathbf{r} \cup \mathbf{r}_c) + \mathcal{T}(\mathbf{r} \cup \mathbf{r}_c, \mathbf{d}_1 \cup \mathbf{d}_{1c}), 1\Big) - \alpha_L/(2\pi) \tag{39}$$

must be zero and we use them as a measure of the error of the algorithms, see figure 7(b).

In Figure 9(a) we plot (38) and (39), for configuration A only, as a function of the number of discretization points N (for the double integral, the closure comprises N/4 additional points). The computation time is given in Figure 9(b). We see that at fixed N the double integral algorithm is approximatively twice more accurate, but requires a computation time several orders of magnitude longer. Finally Figure 9(c), which plots the time required to achieved given accuracy, shows that the Polar Writhe algorithm is more than two orders of magnitude more efficient.

6.2 Case 2: Non Aligned Ends

To showcase the utility of the polar writhe measure we consider a set of curves whose end point joining vector is not aligned with $\hat{\mathbf{z}}$ ($r_x(L) \neq r_x(0)$ and $r_y(L) \neq r_y(0)$), nor have their tangents aligned ($\mathbf{d}_3(L) \neq \mathbf{d}_3(0)$). The rigidities are here also $K_1 = 1.0$, $K_2 = 1.1$, and $K_3 = 1.2$. The $s = 0$ conditions are still given by (36), but the six $s = L(= 1)$ conditions are now given by:

$$r_x(L) = -0.12, \quad r_y(L) = 0.21, \quad r_z(L) = (1 - \Delta)L, \quad d_{3z}(L) = 0.95, \quad d_{1z}(L) = 0, \quad \alpha_L = \bar{\alpha} \tag{40}$$

where α_L (with $0 \leq \alpha_L < 2\pi$) is the rotation angle of $\mathbf{d}_1(L)$ in the basis $(\hat{\mathbf{x}}, \hat{\mathbf{y}})$. We fix $\Delta = 0.72$, and we let $\bar{\alpha}$ evolve from $0.095 \times 2\pi$ to $0.96 \times 2\pi$. We start with a configuration having $\{\mathsf{n}_1(0), \mathsf{n}_2(0), \mathsf{n}_3(0)\} = \{-52.72, 109.65, 93.65\}$ and $\{\mathsf{m}_1(0), \mathsf{m}_2(0), \mathsf{m}_3(0)\} = \{-4.25, -10.68, -9.432\}$ and we select the direction of increasing $\mathsf{m}_3(0)$. The condition $d_{1z}(L) = 0$ imposes the vector $\mathbf{d_1}(L)$ to lie in the $\hat{\mathbf{x}} - \hat{\mathbf{y}}$ plane. The continuation allows the controlled input of winding, i.e increasing $\mathcal{L}_p(\mathbf{r}, \mathbf{v})$, by rotating the vector $\mathbf{d}_1(L)$ in this plane through changing the applied torque $\mathsf{m}_3(0)$, see Figure 10(a).

Typical rod configurations obtained by this continuation are shown in Figure 11, where we see the rod first coils into a left-handed spiral, configuration A. As the angle α_L is increased the rod seems to form two self contacting loops (configuration B), and finally coils into a right-handed spiral (configuration C). The quantities $\mathcal{W}_p^\star$ (computed with $N = 1000$) and $\mathcal{W}(\mathbf{r} \cup \mathbf{r}_c)$ (computed with $N = 1000$ along the curve and $N/4 = 250$ additional points along the closure) are plotted in Figure 10(c) and are virtually indistinguishable.

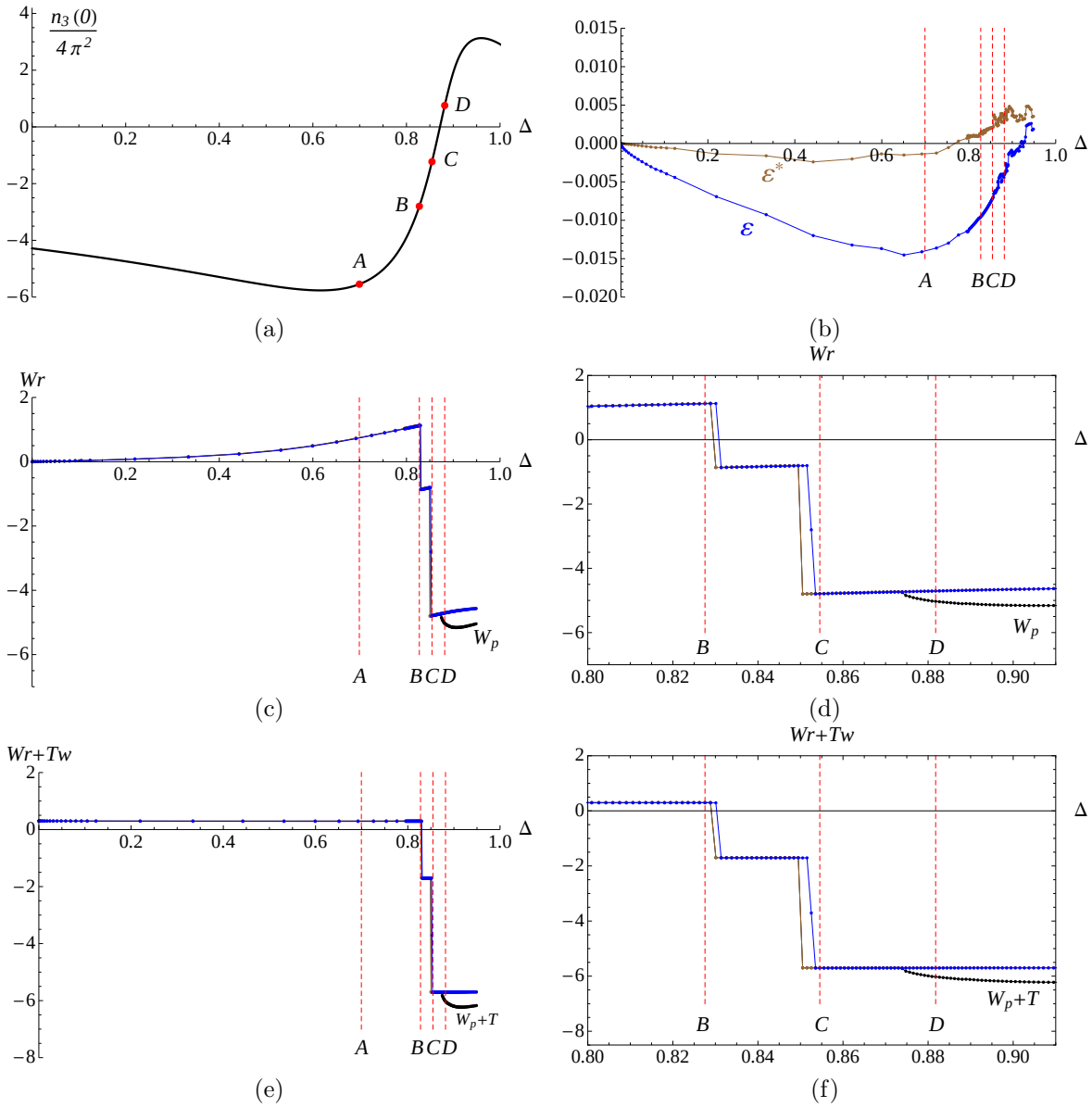

Figure 7: Various plots for case 1. (a) depicts the bifurcation path. (b) shows the errors $\mathcal{E}$ (upper curve) and $\mathcal{E}^\star$ (lower curve). (c) shows the various writhe values as a function of Δ, all values are indistinguishable except near discontinuous jumps and for $\mathcal{W}_p$ where marked. (d) is a zoom of the region of interest in (c). (e) shows sum writhe+twist which is constant for each writhe measure, except near discontinuous jumps and for the sum $\mathcal{W}_p + \mathcal{T}$ where indicated. (f) is a zoom of the region of interest in (e).

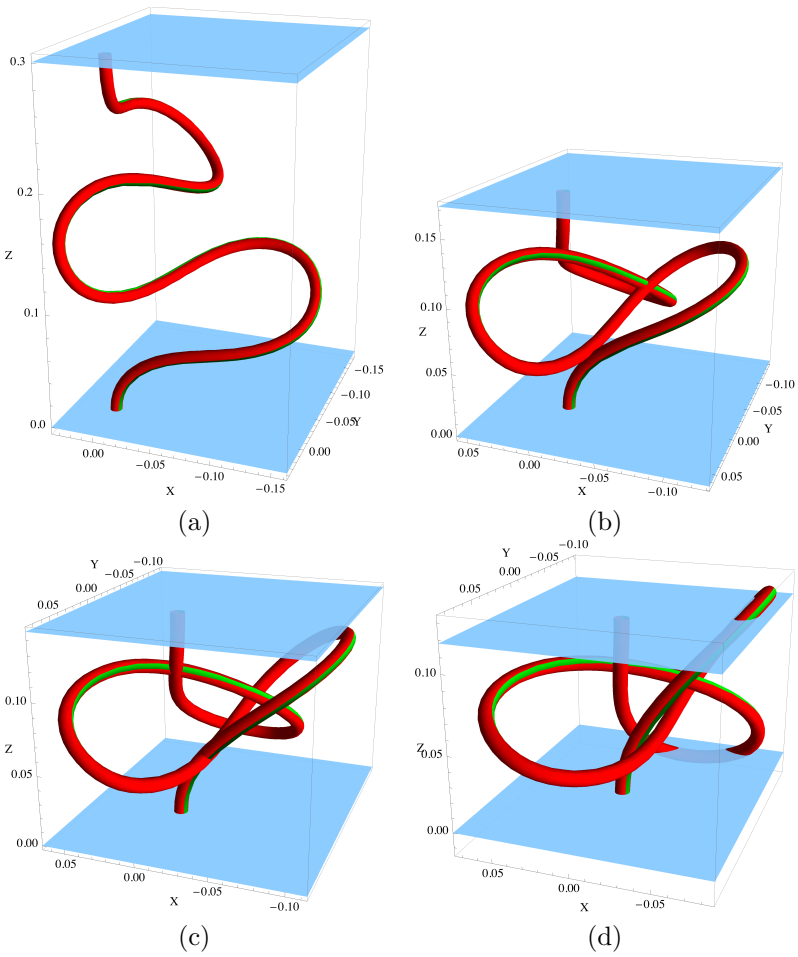

Figure 8: Configurations A, B, C, and D for Case 1. (a) configuration A is prior to any intersections. (b) configuration B is just before a self-intersecting event. (c) configuration C is just after a configuration with two simultaneous intersections. (d) configuration D has a section of the curve above $\mathbf{r}(L)$.

(Please note that as the rod remains within the end-planes, $\mathcal{W}_p = \mathcal{W}_p^\star$). We see that in the vicinity of configuration B the writhe actually jumps twice by + 2 units, i.e two consecutive crossings happen along the bifurcation curve, see Figure 10(d). Configuration B appears to have two crossings because in Figure 11(b) it is rendered with a finite thickness. Finally in Figure 10(b) computation times, for the writhe of configuration C, are plotted as function of the number N of discretization points. These computations were performed in C++ and we see a gain of approximatively two orders of magnitude when compared to the times obtained in Case 1 (see Figure 9(b)) where computations were performed with Mathematica. As in Case 1, the Polar Writhe algorithm is two (or more) orders of magnitude quicker than the classical double integral algorithm [47], and approximatively two times quicker than the algorithm from [1].

6.3 Case 3: An Unknotting Deformation

To demonstrate the detection of a change in (pulled-tight) topology we consider a bifurcation path where a section of the curve gradually loops over the $s = L$ end of the curve. Here we choose the end tangents to be parallel but the curves end-points to be non aligned, that is the $s = 0$ conditions are given by (36) and the six $s = L(= 1)$ conditions are:

$$r_x(L) = 0.0397, \quad r_y(L) = -0.0304, \quad r_z(L) = (1 - \Delta)L, \quad d_{3z} = 1, \quad d_{1z} = 0, \quad \alpha_L = \bar{\alpha} \tag{41}$$

where α_L (with $0 \leq \alpha_L < 2\pi$) is the rotation angle of $\mathbf{d}_1(s = L)$ in the basis $(\hat{\mathbf{x}}, \hat{\mathbf{y}})$. Please also note that here we choose $K_1 = 1$, $K_2 = 3 = K_3$. We fix $\Delta = 0.85$, and we let $\bar{\alpha}$ evolve from 5.01 to 4.95. We

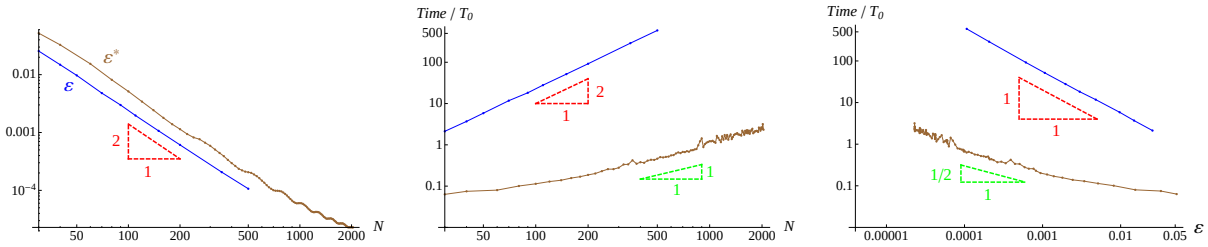

Figure 9: Plots detailing the convergence and timing of the various algorithms for configuration A of Case 1. (a) shows that the error is decreasing as $1/N^2$ for both the $\mathcal{W}_p^\star$ (upper curve) and $\mathcal{W}(\mathbf{r} \cup \mathbf{r}_c)$ (lower curve) algorithms. (b) shows, as a function or N, the time needed for the algorithms to compute $\mathcal{W}_p^\star$ (lower curve, scaling $N^{1.0}$) and $\mathcal{W}(\mathbf{r} \cup \mathbf{r}_c)$ (upper curve, scaling N^2). (c) gives the time needed to achieve a certain accuracy, using the $\mathcal{W}_p^\star$ (lower curve) and $\mathcal{W}(\mathbf{r} \cup \mathbf{r}_c)$ (upper curve) algorithms. Computations were performed in Mathematica 8.

start with a configuration having $\{\mathsf{n}_1(0), \mathsf{n}_2(0), \mathsf{n}_3(0)\} = \{-27.55, 20.41, 45.15\}$ and $\{\mathsf{m}_1(0), \mathsf{m}_2(0), \mathsf{m}_3(0)\} = \{6.505, -9.425, 4.941\}$ and we select the direction of increasing $\mathsf{m}_3(0)$. Once again the condition $d_{1z} = 0$ forces the vector $\mathbf{d_1}$ to lie in the $\hat{\mathbf{x}} - \hat{\mathbf{y}}$ plane and we control the changing $\mathcal{L}_p(\mathbf{r}, \mathbf{v})$ value by rotating the vector $\mathbf{d}_1(L)$ (changing $\bar{\alpha}$) through changing the torque $\mathsf{m}_3(0)$. Figure 12 shows a plot of the quantities $\mathcal{W}(\mathbf{r} \cup \mathbf{r}_c)$, $\mathcal{W}_p^\star$, and $\mathcal{W}_p$ as a function of $\mathsf{m}_3(0)$ while four configurations along the path are shown in Figure 13. The closure $\mathbf{r}_c$ used for $\mathcal{W}(\mathbf{r} \cup \mathbf{r}_c)$ is shown in Figure 13, we draw the readers attention to the fact that the looped section will cross this closure before it crosses the $\mathcal{W}_p^\star$ extension. Initially the writhe values are virtually indistinguishable, near 3.5 a value one might expect for a trefoil knot. In configuration A the entire curve $\mathbf{r}(s)$ lies between the bounding planes, and the three writhe values coincide. As $\mathsf{m}_3(0)$ is increased, a looped section of the curve rises above the upper plane (see for example configuration B) and $\mathcal{W}_p$ now departs from the other two writhe values, decreasing almost linearly as the looping occurs, confirming what we would expect from Figure 6(b). Along the deformation path, the looped section never goes back down below the upper plane and hence we have $\mathcal{W}_p \neq \mathcal{W}_p^\star$. Then, between configurations B and C, the curve $\mathbf{r}(s)$ crosses the closure $\mathbf{r}_c(t)$ and the $\mathcal{W}(\mathbf{r} \cup \mathbf{r}_c)$ value jumps by two units. Eventually, between configurations C and D, the curve crosses the straight extension above point $\mathbf{r}(L)$ and the $\mathcal{W}_p^\star$ value jumps by two units, recovering the value given by $\mathcal{W}(\mathbf{r} \cup \mathbf{r}_c)$. In conclusion we see that the choice of the closure in the computation of $\mathcal{W}(\mathbf{r} \cup \mathbf{r}_c)$ as well as the choice of the extension curve in the computation of $\mathcal{W}_p^\star$ can play crucial roles splitting open ribbon configurations into distinct topological domains.

6.4 Discussion

We see the error and convergence of the three algorithms are very similar. The algorithm for $\mathcal{W}_p^\star$ is the quickest algorithm. However, the main advantage in the polar writhe formulation is the absence of closure. For the particular examples used here the closures were relatively simple and crucially quite small so they did not require too many points for accurate calculations. The most general closures introduced in the following section can be significantly large and their contribution to the quantity $\mathcal{W}(\mathbf{r} \cup \mathbf{r}_c)$ **must** be calculated for accurate evaluations. This could require a much larger number of points in the most general case. Moreover the specific form the closure takes must always be explicitly quantified, making a general code hard to design. The quantity $\mathcal{W}_p^\star$ **never** requires a closure for calculation so this is never an issue and a code which covers all admissible cases is already available [supplementary material].

6.5 Conclusion

In conclusion we have illustrated how the Călugăreanu theorem can be extended to open ribbons using quantities called the polar writhe and the net-winding, quantities formerly introduced in [12]. We have extended the definition of these quantities to cope with cases where the curve has sections that cross the bounding planes such as knotting and belt-trick deformations.

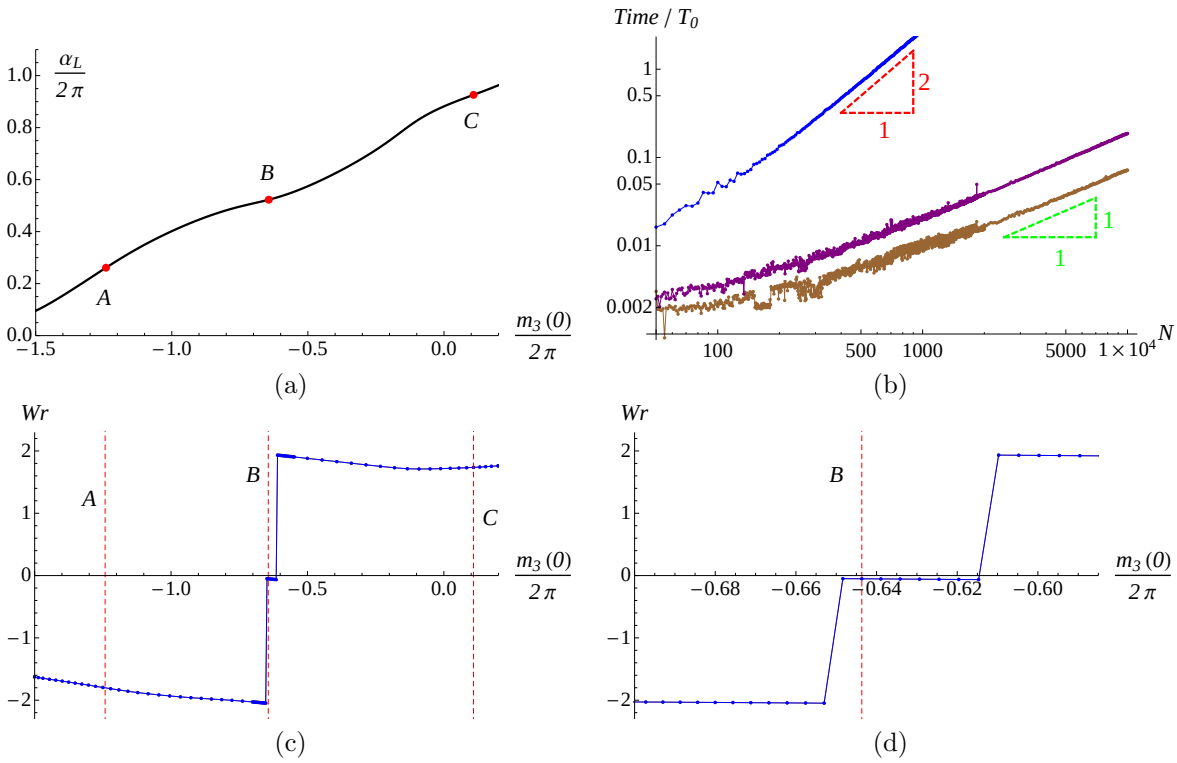

Figure 10: Various plots for Case 2. (a) displays the bifurcation path. (b) shows the computation time for the algorithms for $\mathcal{W}_p^\star$ (lower curve), the algorithm for $\mathcal{W}(\mathbf{r} \cup \mathbf{r}_c)$ from [1] (intermediate curve), and the algorithm for $\mathcal{W}(\mathbf{r} \cup \mathbf{r}_c)$ from [47] (upper curve). (c) depicts the values of $\mathcal{W}(\mathbf{r} \cup \mathbf{r}_c)$ and $\mathcal{W}_p^\star$ as function of $\mathsf{m}_3(0)$ (the values are almost indistinguishable). The writhe has two jumps and configuration labelled B is after the first jump and before the second. Computations were performed in C++.

We have also introduced an algorithm to compute the extended polar writhe and we have shown, on selected examples curves arising in the study of elastic rods mechanics, the efficiency of the algorithm when compared to existing algorithms for computing the double-integral writhe.

7 Acknowledgments

We thank Yusu Wang (Ohio State University) for providing us with the code introduced in [1]. S.N. acknowledges support from the Royal Society, through the International Exchanges Scheme (grant IE120203). C.P. acknowledges funding from an Addison Wheeler fellowship.

References

[1] Pankaj K. Agarwal, Herbert Edelsbrunner, and Yusu Wang. Computing the writhing number of a polygonal knot. *Discrete & Computational Geometry*, 32(1):37–53, 2004.

[2] Jürgen Aldinger, Isaac Klapper, and Michael Tabor. Formulae for the calculation and estimation of writhe. *Journal of Knot theory and its Ramifications*, 4(03):343–372, 1995.

[3] J.C. Alexander and Stuart S. Antman. The ambiguous twist of love. *Quarterly of Applied Mathematics*, 40(1):83–92, 1982.

[4] Stuart S. Antman. *Nonlinear problems of elasticity*. Springer, 2005.

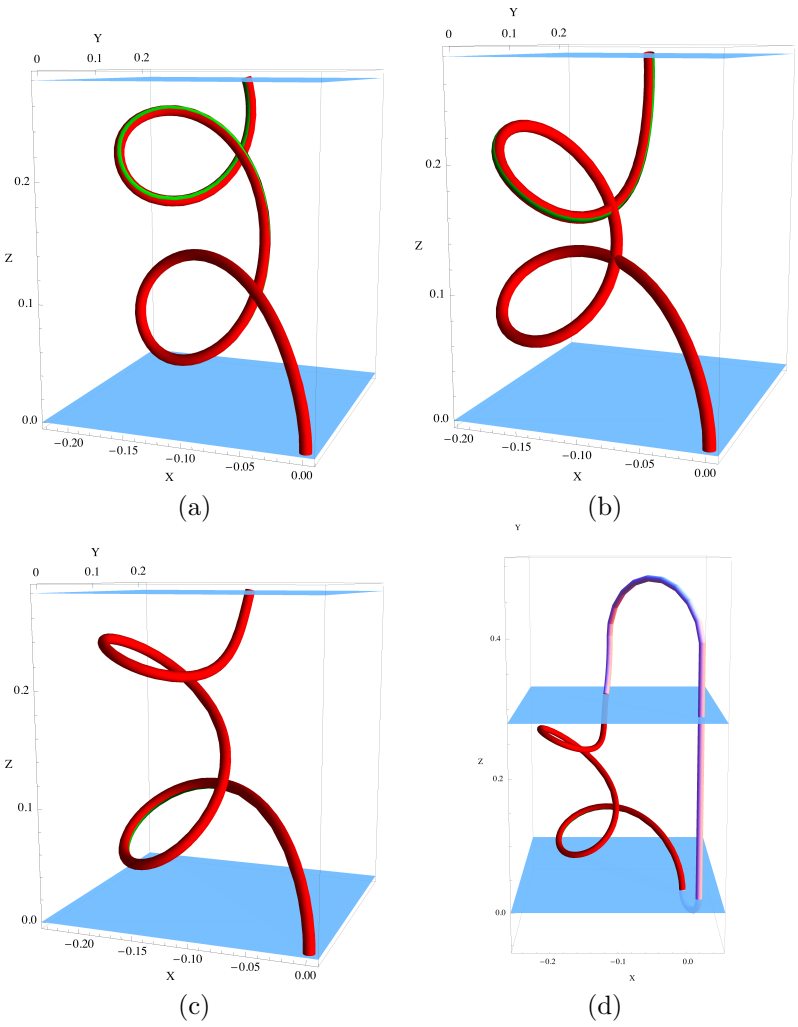

Figure 11: Configurations A B and C for Case 2. (a) configuration A is a left-handed coil, (b) configuration B resembles two self-crossing loops, while (c) configuration C is a right-handed coil. (d) For configuration C, the closure $\mathbf{r}_c$ used to compute $\mathcal{W}(\mathbf{r} \cup \mathbf{r}_c)$ is shown together with the curve $\mathbf{r}$.

[5] VI Arnold. Ordinary differential equations, translated by ra silverman. *MIT Press, Cambridge, Massachusetts*, 2:196–213, 1973.

[6] Mahboubeh Asgari-Targhi and Mitchell A. Berger. Writhe in the stretch-twist-fold dynamo. *Geophysical and Astrophysical Fluid Dynamics*, 103(1):69–87, 2009.

[7] Basile Audoly and Yves Pomeau. *Elasticity and Geometry*. Oxford Univ. Press, 2010.

[8] Alexander Balaeff, L. Mahadevan, and Klaus Schulten. Elastic rod model of a DNA loop in the lac operon. *Physical Review Letters*, 83(23):4900–4903, 1999.

[9] Meriem Baouendi, Jean A. H. Cognet, Catia S. M. Ferreira, Sotiris Missailidis, Jérome Coutant, Martial Piotto, Edith Hantz, and Catherine Hervé du Penhoat. Solution structure of a truncated anti-MUC1 DNA aptamer determined by mesoscale modeling and NMR. *FEBS Journal*, 279(3):479–490, 2012.

[10] Richard A Battye and Paul M Sutcliffe. Knots as stable soliton solutions in a three-dimensional classical field theory. *Physical Review Letters*, 81(22):4798, 1998.

[11] Craig J Benham. Elastic model of supercoiling. *Proceedings of the National Academy of Sciences of the USA*, 74(6):2397–2401, 1977.

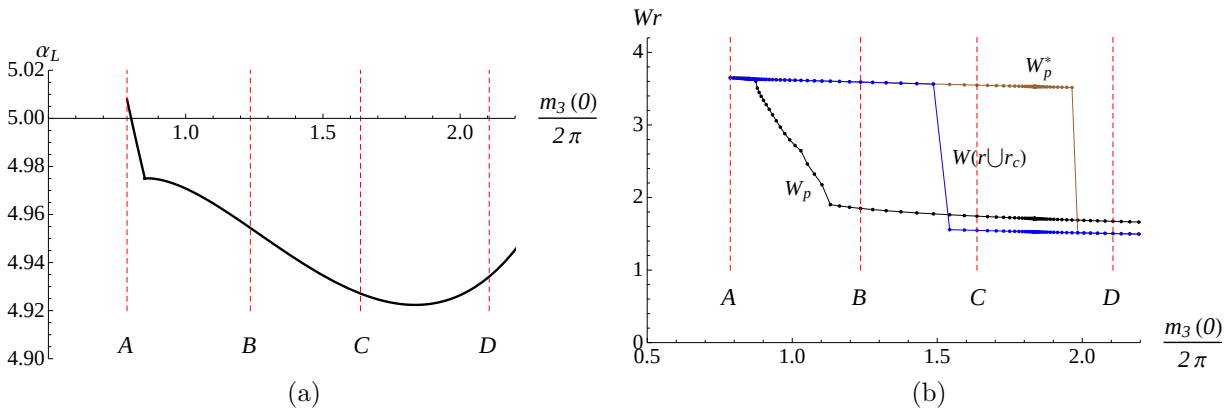

Figure 12: Plots for Case 3. (a) displays the bifurcation path. (b) The writhe measures $\mathcal{W}_p$, $\mathcal{W}_p^\star$, and $\mathcal{W}(\mathbf{r} \cup \mathbf{r}_c)$ are plotted as functions of the torque. Labels A, B, C, and D correspond to the configurations in Figure 13. The value given by $\mathcal{W}_p$ departs for the other two as soon as the configuration extends over the upper plane. The value $\mathcal{W}(\mathbf{r} \cup \mathbf{r}_c)$ jumps as the configuration crosses the closure. The value given by $\mathcal{W}_p^\star$ jumps when the extension is crossed.

[12] Mitchell A Berger and Chris Prior. The writhe of open and closed curves. *Journal of Physics A: Mathematical and General*, 39(26):8321, 2006.

[13] Richard L. Bishop. There is more than one way to frame a curve. *American Mathematical Monthly*, pages 246–251, 1975.

[14] Claude Bouchiat and Marc Mezard. Elastic rod model of a supercoiled DNA molecule. *The European Physical Journal E*, 2(4):377–402, 2000.

[15] Carlos Bustamante, Zev Bryant, and Steven B. Smith. Ten years of tension: single-molecule DNA mechanics. *Nature*, 421(6921):423–427, 2003.

[16] George Călugăreanu. L'intégrale de Gauss et l'analyse des nœuds tridimensionnels. *Rev. Math. Pures Appl*, 4(5), 1959.

[17] George Călugăreanu. Sur les classes d'isotopie des nœuds tridimensionnels et leurs invariants. *Czechoslovak Mathematical Journal*, 11(4):588–625, 1961.

[18] B Ruiz Cobo and Klaus G Puschmann. Twist, writhe, and helicity in the inner penumbra of a sunspot. *The Astrophysical Journal*, 745(2):141, 2012.

[19] Bernard D Coleman and David Swigon. Theory of supercoiled elastic rings with self-contact and its application to DNA plasmids. *Journal of elasticity and the physical science of solids*, 60(3):173–221, 2000.

[20] James Coyne. Analysis of the formation and elimination of loops in twisted cable. *IEEE Journal of Oceanic Engineering*, 15(2):72–83, 1990.

[21] Boris Fain, Joseph Rudnick, and Stellan Östlund. Conformations of linear DNA. *Physical Review E*, 55(6):7364, 1997.

[22] F Brock Fuller. Decomposition of the linking number of a closed ribbon: a problem from molecular biology. *Proceedings of the National Academy of Sciences of the USA*, 75(8):3557–3561, 1978.

[23] Alain Goriely and Michael Tabor. Spontaneous helix hand reversal and tendril perversion in climbing plants. *Physical Review Letters*, 80(7):1564, 1998.

[24] Y Guo, MD Ding, X Cheng, J Zhao, and E Pariat. Twist accumulation and topology structure of a solar magnetic flux rope. *The Astrophysical Journal*, 779(2):157, 2013.

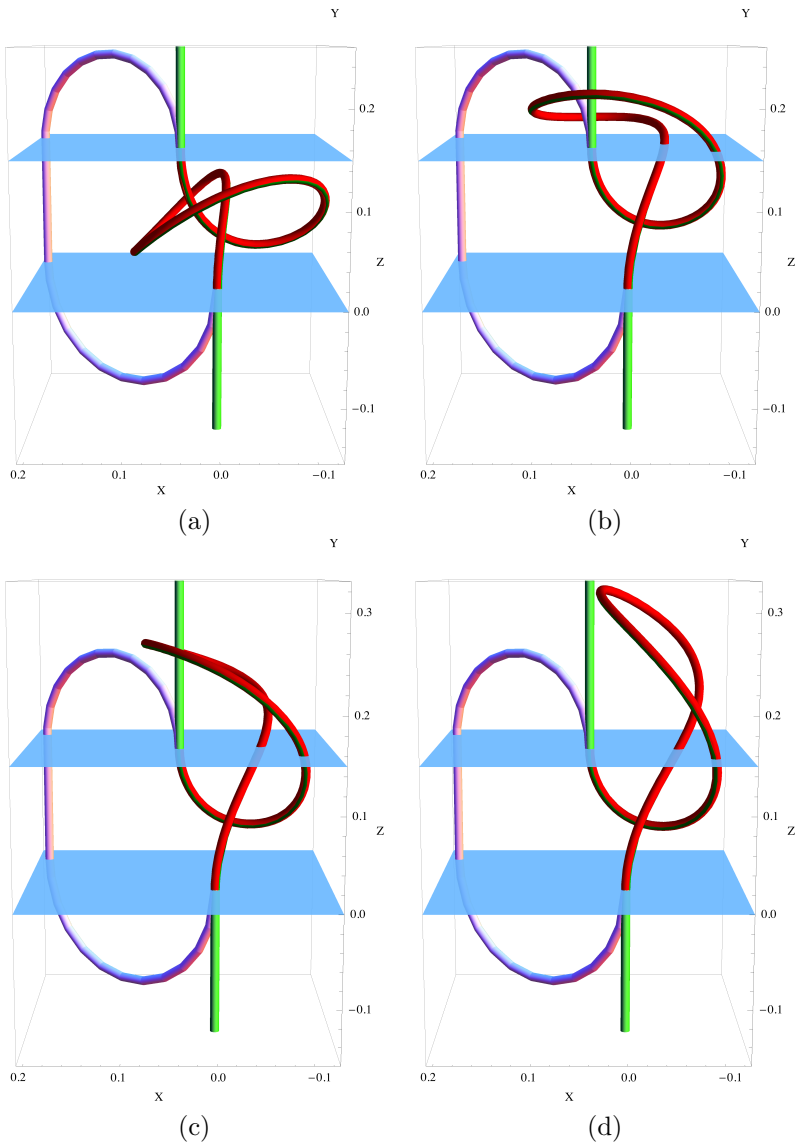

Figure 13: The four configurations corresponding to points A (a), B (b), C (c), and D (d) in Figure 12 for the unknotting deformation path considered in Case 3. In (a) configuration A entirely lies between the end planes and is essentially knotted. In (b) configuration B has a looped section above the upper plane and consequently $\mathcal{W}_p^\star \neq \mathcal{W}_p$. In (c) the looped section of configuration C has just crossed the closure $\mathbf{r}_c$ and consequently $\mathcal{W}_p^\star \neq \mathcal{W}(\mathbf{r} \cup \mathbf{r}_c)$. In (d) configuration D has just crossed the straight extension of the curve above the point $\mathbf{r}(L)$. The value $\mathcal{W}_p^\star$ has jumped by -2 units and we have $\mathcal{W}_p^\star = \mathcal{W}(\mathbf{r} \cup \mathbf{r}_c)$ back again.

[25] Derek Harland, Martin Speight, and Paul Sutcliffe. Hopf solitons and elastic rods. *Physical Review D*, 83(6):065008, 2011.

[26] Morris W Hirsch. *Differential topology*. Springer, 1976.

[27] S Inoue, D Shiota, TT Yamamoto, VS Pandey, T Magara, and GS Choe. Buildup and release of magnetic twist during the x3.4 solar flare of 2006 december 13. *The Astrophysical Journal*, 760(1):17, 2012.

[28] ÅM Janse and BC Low. The topological changes of solar coronal magnetic fields. III. reconnected field topology produced by current-sheet dissipation. *The Astrophysical Journal*, 722(2):1844, 2010.

[29] Konstantin Klenin and Jörg Langowski. Computation of writhe in modeling of supercoiled DNA. *Biopolymers*, 54(5):307–317, 2000.

[30] Arnaud Lazarus, Jay T. Miller, Matthew M. Metlitz, and Pedro M. Reis. Contorting a heavy and naturally curved elastic rod. *Soft Matter*, 9:8274–8281, 2013.

[31] DW Longcope and I Klapper. Dynamics of a thin twisted flux tube. *The Astrophysical Journal*, 488(1):443, 1997.

[32] BC Low. Absolute magnetic helicity and the cylindrical magnetic field. *Physics of Plasmas*, 18(5):052901, 2011.

[33] BC Low. Newtonian and non-newtonian magnetic-field relaxations in solar-coronal MHD. *The Astrophysical Journal*, 768(1):7, 2013.

[34] Francesca Maggioni and Renzo L Ricca. Writhing and coiling of closed filaments. *Proceedings of the Royal Society A: Mathematical, Physical and Engineering Science*, 462(2074):3151–3166, 2006.

[35] R.S. Manning, J.H. Maddocks, and J.D. Kahn. A continuum rod model of sequence-dependent DNA structure. *J. Chem. Phys.*, 105:5626–5646, 1996.

[36] John F. Marko and Simona Cocco. The micromechanics of DNA. *Physics World*, pages 37–41, 2003.

[37] Sébastien Neukirch, Alain Goriely, and Andrew Hausrath. Chirality of coiled-coils: elasticity matters. *Physical Review Letters*, 100:038105, 2008.

[38] Sébastien Neukirch and Eugene L Starostin. Writhe formulas and antipodal points in plectonemic DNA configurations. *Physical Review E*, 78(4):041912, 2008.

[39] William F Pohl. The self-linking number of a closed space curve (Gauss integral formula treated for disjoint closed space curves linking number). *Journal of Mathematics and Mechanics*, 17:975–985, 1968.

[40] C Prior. *The theory and applications of writhing*. PhD thesis, UCL, 2010.

[41] C Prior and MA Berger. On the shape of force-free field lines in the solar corona. *Solar Physics*, 278(2):323–345, 2012.

[42] C Prior and AR Yeates. On the helicity of open magnetic fields. *The Astrophysical Journal*, 787(2):100, 2014.

[43] Vincent Rossetto and AC Maggs. Writhing geometry of open DNA. *The Journal of chemical physics*, 118(21):9864–9874, 2003.

[44] Yaoming Shi and John E Hearst. The kirchhoff elastic rod, the nonlinear schrödinger equation, and DNA supercoiling. *The Journal of chemical physics*, 101(6):5186–5200, 1994.

[45] Steven B Smith, Laura Finzi, and Carlos Bustamante. Direct mechanical measurements of the elasticity of single DNA molecules by using magnetic beads. *Science*, 258(5085):1122–1126, 1992.

[46] E. L. Starostin. On the writhing number of a non-closed curve. In J. A. Calvo, K. C. Millett, E. J. Rawdon, and A. Stasiak, editors, *Physical and Numerical Models in Knot Theory Including Applications to the Life Sciences*, volume 36 of *Series on Knots and Everything*, chapter 26, pages 525–545. World Scientific, 2005.

[47] David Swigon, Bernard D Coleman, and Irwin Tobias. The elastic rod model for DNA and its application to the tertiary structure of DNA minicircles in mononucleosomes. *Biophysical journal*, 74(5):2515–2530, 1998.

[48] J Brian Taylor. Relaxation of toroidal plasma and generation of reverse magnetic fields. *Physical Review Letters*, 33(19):1139, 1974.

[49] Tibor Toeroek, Mitchell A Berger, and Bernhard Kliem. The writhe of helical structures in the solar corona. *arXiv preprint arXiv:1004.3918*, 2010.

[50] T Török, Bernhard Kliem, Mitchell A Berger, Mark G Linton, Pascal Demoulin, and Lidia van Driel-Gesztelyi. The evolution of writhe in kink-unstable flux ropes and erupting filaments. *Plasma Physics and Controlled Fusion*, 56(6):064012, 2014.

[51] GHM Van der Heijden, Mark A Peletier, and Robert Planqué. On end rotation for open rods undergoing large deformations. *Quarterly of applied mathematics*, 65(2):385, 2007.